

Frequency Response Analysis of a Current Limiting Reactor

Levashen Kuppan

Electrical Engineering

Date: 21/04/2022

In fulfilment of the Masters of Science, College of Agriculture, Engineering and Science, University of KwaZulu-Natal

Supervisor: Dr Andrew G. Swanson

Co-supervisor: Dr A. L. Leigh Jarvis

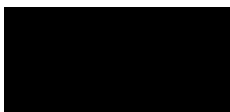
COLLEGE OF AGRICULTURE, ENGINEERING AND SCIENCE

DECLARATION 1 - PLAGIARISM

I, Levashen Kuppan, declare that

1. The research reported in this thesis, except where otherwise indicated, is my original research.
2. This thesis has not been submitted for any degree or examination at any other university.
3. This thesis does not contain other persons' data, pictures, graphs or other information, unless specifically acknowledged as being sourced from other persons.
4. This thesis does not contain other persons' writing, unless specifically acknowledged as being sourced from other researchers. Where other written sources have been quoted, then:
 - a. Their words have been re-written but the general information attributed to them has been referenced
 - b. Where their exact words have been used, then their writing has been placed in italics and inside quotation marks, and referenced.
5. This thesis does not contain text, graphics or tables copied and pasted from the Internet, unless specifically acknowledged, and the source being detailed in the thesis and in the References sections.

Student Signature



Supervisor Signature

Acknowledgments

I would like to express my deep and sincere gratitude to my research supervisor, Dr Andrew G. Swanson, who has continuously been of immense and support throughout the writing of this dissertation. Your guidance, patience and vision has helped take my skill set to new levels and it has been a great privilege to study under your supervision.

Finally, I would like to thank my family and friends who have supported me throughout my studies and motivated me to reach my goals.

Abstract

With the demand for electricity continuously increasing, power systems are required to increase capacity to meet such demands which can entail integrating renewable energy resources to the grid. This increase in capacity would mean a likewise increase in fault levels in the network which can result in costly damage to components such as circuit breakers, transformers and cables. Air-core reactors are commonly employed to prevent such damages from occurring, however, the increase in fault levels must also be accounted for in the design of reactors as they are also subject to transients.

This dissertation documents the development of models to accurately represent an Air-core reactor in order to gain a better understanding of the design considerations required. Two models are developed for two desktop reactors using different methods as a form of cross-validation. The first model is developed in MATLAB r2020a and utilises an analytical approach through an equivalent circuit method (ECM). Equations are used to compute the inductive, capacitive and resistive components which are then used to guide the development of the FEM models. The second model is developed using COMSOL Multiphysics software which is based on the Finite Element Method (FEM) approach. A 2D-axisymmetrical model is constructed and simulated using COMSOL's Magnetic and Electric field physics in the frequency domain from which a frequency response is obtained as well as values for the inductive, resistive and capacitive components. Final validation of the FEM models is done through comparisons to measured results of the two desktop reactors. FEM simulated RLC components showed fairly good agreement to the measured values, particularly the inductance having a difference of 3.4 μH and a capacitance difference of 1 pF for Reactor 1. The FEM simulated frequency response of 1.5 MHz differed by 0.4 MHz when compared to the measured frequency response for Reactor 2 of 1.9 MHz.

A sensitivity analysis is conducted for the FEM model in order to obtain an understanding of the design considerations required for the air-core reactor. Simulations are performed on the FEM model with changes to geometry, permittivity of the insulation medium and resistivity of the copper coil. The effects of these changes on the RLC parameters and resonance frequencies are documented.

The FEM model is then scaled to a full-scaled reactor which showed good agreement between the expected inductance of 2.24 mH and the simulated inductance of 2.28 mH. The resultant resonant frequency was observed to occur at 380 kHz.

The aim of this is to develop an understanding of parameters and equations that should be considered in the design process of reactors which will then be employed in the development of a superconducting fault current limiter (SFCL).

Contents

Abstract.....	iii
List of Figures.....	vii
List of Tables.....	ix
Acronyms.....	x
1 Introduction.....	1
1.1 Research Question.....	2
1.2 Importance of Study and Contribution.....	2
1.2.1 Limitations of the Research.....	2
1.3 Dissertation Structure.....	2
2 Literature Review.....	4
2.1 Background Theory on Current Limiting Reactors.....	4
2.1.1 Types of Fault Current Limiting Reactors.....	4
2.1.2 Dry-type vs Oil-immersed.....	5
2.1.3 Structure of an Air-core Reactor.....	5
2.1.4 Structure of a Coolant Immersed Reactor.....	6
2.1.5 Installation Locations of Current Limiting Reactors (CLRs).....	6
2.1.6 Other Applications of Air-core Reactors in Power Systems.....	8
2.2 Transient Voltages.....	9
2.3 Electromagnetic Behaviour of a Reactor.....	9
2.3.1 Capacitive Component.....	10
2.3.2 Inductive Component.....	12
2.3.3 Resistance of a Solenoid.....	14
2.3.4 Skin and Proximity Effects.....	15
2.3.5 Frequency Response.....	15
2.4 Modelling Methodologies.....	17
2.4.1 Transmission Line Modelling.....	17
2.4.2 Lumped Parameter Circuit Model.....	18
2.4.3 Partial Element Equivalent Circuit (PEEC).....	19

2.4.4	Finite Element Method (FEM).....	19
2.4.5	Summary of Modelling Methodologies	20
3	Reactor Models	21
3.1	Equivalent Circuit Model.....	22
3.1.1	Inductance Calculations	22
3.1.2	Capacitance Calculations	22
3.1.3	Resistance Calculations.....	22
3.1.4	Resonance Frequency Calculations.....	23
3.2	Finite Element Model	23
3.2.1	Geometry.....	23
3.2.2	Materials	24
3.2.3	Physics	25
3.2.4	Mesh Settings.....	26
3.2.5	FEM Results Reactor 1	28
3.2.6	FEM Results Reactor 2	31
4	Measurements of Reactor.....	35
4.1	Reactor 1 Measurements.....	35
4.1.1	Laboratory Setup.....	35
4.1.2	Measured Quantities	35
4.2	Reactor 2 Measurements.....	36
4.2.1	Measurement System for the Impedance Measurement	36
4.2.2	Device Description.....	36
4.2.2.3	GW Instek AFG	37
4.2.3	Device Specifications.....	38
4.2.4	Results.....	39
4.3	Validation of models.....	42
5	Sensitivity Analysis of the Reactor Model.....	45
5.1	Geometrical Sensitivity Analysis.....	45
5.1.1	Length (z scaling).....	45

5.1.2	Width (r scaling)	46
5.1.3	Summary of Geometrical Sensitivity Analysis	47
5.2	Liquid Nitrogen Insulation	48
5.3	Resistivity of Copper	49
5.4	Full-Scale Reactor Geometry	53
5.5	FEM Simulation Results	54
6	Conclusion	55
6.1	Recommendations	56
7	References	57
	Appendix A1 – Extra-coarse mesh	60
	Appendix A2 – Normal mesh	60
	Appendix A3 – Extra-fine mesh	61
	Appendix A4 – Extremely-fine mesh	61
	Appendix B1 – Capacitance of cable for measurements	62
	Appendix B2 – Capacitance of desktop reactor	62
	Appendix B3 – Resistance measurement for the desktop reactor	63
	Appendix B4 – Phase angle measurement for the desktop reactor	63
	Appendix C – MATLAB code RLC calculations	64
	Appendix D – MATLAB code SFRA	65

List of Figures

Figure 1: Cross-section of a basic air-core dry-type reactor	5
Figure 2: Generator reactors in a network	6
Figure 3: Feeder reactors in a network.....	7
Figure 4: Bus-bar reactors in a network (ring system).....	7
Figure 5: Tie-bar reactors in a network.....	8
Figure 6: Circuit representation of an air-core reactor coil.....	10
Figure 7: Basic diagram explaining capacitance between planes	10
Figure 8: Cross-sectional view of two turns in a reactor	11
Figure 9: Cross-sectional view of two coaxial coils	13
Figure 10: Cross-sectional view of a solenoid	14
Figure 11: Equivalent lumped circuit of an inductor	16
Figure 12: Frequency response of a single phase transformer [17]	17
Figure 13: Desktop Reactor 1	21
Figure 14: Desktop Reactor 2	21
Figure 15: Full geometrical structure representing Air-core reactor in 2d-axisymmetrical plain.....	23
Figure 16: 3D visual of constructed Air-core reactor model	24
Figure 17: Components of structure labelled with corresponding materials	24
Figure 18: RLC coil group governed by Ampere's law.....	25
Figure 19: Magnetic insulation boundary	26
Figure 20: Mesh setting effects on resonance frequency	28
Figure 21: Frequency response of COMSOL model showing Impedance vs Frequency for Reactor 129	
Figure 22: Corresponding Phase vs Frequency for COMSOL model for Reactor 1	29
Figure 23: Zoomed resonance peak for Reactor 1 frequency response	30
Figure 24: Electric field at 1kHz for Reactor 1	31
Figure 25: Electric potential at 1kHz for Reactor 1	31
Figure 26: Frequency response of COMSOL model showing Impedance vs Frequency for Reactor 232	
Figure 27: Corresponding Phase vs Frequency for COMSOL model for Reactor 2	32
Figure 28: Zoomed resonance peak for Reactor 2 frequency response	33
Figure 29: Electric field at 1kHz for Reactor 2.....	33
Figure 30: Electric potential at 1kHz for Reactor 2	34
Figure 31: Inductance measurement of the desktop reactor.....	35
Figure 32: Measurement system for impedance measurement	36
Figure 33: Red Pitaya device	37
Figure 34: GW Instek AFG.....	38
Figure 35: Comparison of frequency responses for Reactor 2.....	39

Figure 36: Experiment 1 setup using Red Pitaya	40
Figure 37: Experiment 3 setup showing the Red Pitaya and AFG combination.....	40
Figure 38: Red Pitaya VNA module connected to the Red Pitaya	41
Figure 39: Modified measurement system for impedance measurement.....	41
Figure 40: Experiment 4 setup for VNA.....	42
Figure 41: Frequency response and phase comparison between the COMSOL model and VNA measurement for Reactor 2	44
Figure 42: frequency response – z scaling	45
Figure 43: Frequency response - z scaling resonant frequency peak zoom	46
Figure 44: frequency response – r scaling	46
Figure 45: Frequency response - r scaling resonant frequency peak zoom	47
Figure 46: Frequency response comparison - liquid nitrogen.....	48
Figure 47: Frequency response comparison - liquid nitrogen resonant frequency zoom	49
Figure 48: Impedance comparison for $T = 300 \text{ K}$ and $T = 77 \text{ K}$	50
Figure 49: Comparison of approximate effect of conductivity on current density	51
Figure 50: Comparison of current density where (a) $T = 300 \text{ K}$ and (b) $T = 77 \text{ K}$	52
Figure 51: FEM geometry for full scale reactor.....	53
Figure 52: Impedance frequency response of the full-scale reactor.....	54

List of Tables

Table 1: Dimensions of the desktop reactor.....	21
Table 2: Calculated Inductance values for Reactor 1 and 2.....	22
Table 3: Capacitance values computed using MATLAB	22
Table 4: Calculated resistance values for Reactor 1 and 2.....	23
Table 5: Calculated resonance frequencies.....	23
Table 6: Table of material properties for FEM model	24
Table 7: Mesh sensitivity analysis at 1kHz for Reactor 1	27
Table 8: Reactor parameters at 1kHz for Reactor 1	30
Table 9: Reactor parameters at 1 kHz for Reactor 2.....	34
Table 10: Table of recorded parameters for desktop reactor 1	36
Table 11: Detailed specifications of measurement devices	38
Table 12: Legend description.....	39
Table 13: Table of RLC parameters for Reactor 1 comparing measured, FEM and ECM models	43
Table 14: Table of RLC parameters for Reactor 2 comparing FEM and ECM models.....	43
Table 15: Table comparing FEM resonance frequencies to calculated resonance frequencies	43
Table 16: RLC parameters at 1 kHz for structural scaling of reactor	47
Table 17: Table of dimensions of a full scale reactor	53
Table 18: FEM results for a full-scaled reactor at 1 kHz.....	54

Acronyms

FEM	Finite Element Method
ECM	Equivalent Circuit Method
PEEC	Partial Element Equivalent Circuit
STL/MTL	Single/Multi-conductor Transmission Line
CLR	Current Limiting Reactor
SFCL	Superconducting Fault Current Limiter
SSR	Superconducting Series Reactor

1 Introduction

In medium voltage (MV) networks, switching may occur regularly which would mean fault currents occurring more frequently in the network. This would call for a fail-safe solution that is reliable enough for constant switching. Devices such as circuit breakers, high impedance transformers, fault current limiters and current limiting reactors (CLRs) are commonly employed to reduce the effects of fault currents and provide the necessary protection to prevent damage to equipment in the network. Current limiting reactors are commonly employed for such situations due to their reliability and simple implementation in networks to mitigate the requirement of further upgrades to existing equipment in the network for increased fault currents. During normal operations, the reactor would allow current to flow and when a large fault current occurs, the impedance of the reactor would increase sharply, thereby reducing the fault current to a level that the components in the network can safely handle.

It was proposed by Khan et al. [1] to design and test a superconducting series reactor (SSR) as this would reduce ohmic losses. They developed a desktop SSR as well as an equivalent copper based reactor for comparison purposes. The reactors were shown to be effective, with the SSR having a lower resistance resulting in fewer ohmic losses. This led them to propose and designed a full scale SSR for installation on 11 kV or 22 kV networks. Instead of conventional conductor wire, the superconductor reactor was based on high temperature superconductor tape. Working with tape adds a level of handling and working complexity. The high temperature superconductor material ($Y_1Ba_2Cu_3O_{7-x}$) enabled use of cheap cryogen, liquid nitrogen. The SSR was enclosed in a stainless-steel tank filled with liquid nitrogen with a suitable thermal insulation. This would add an additional capacitive component for the installation and may change the voltage distribution in the winding for transients that occur on the power system due to switching operations, lightning overvoltages and other voltage abnormalities.

Air-core reactors introduce losses to the network during normal operations mainly due to its resistance. This resistance can be reduced by lowering the temperature of the copper winding in the reactor during normal operations. Reducing the resistivity may reduce the damping effects for any resonances that occur in the device.

Various modelling methodologies have been done in the past for air-core reactors such as circuit analysis, finite element modelling, transmission line modelling, etc., which are further discussed in Chapter 2. This dissertation contributes to the design and development of the SSR by studying the frequency response of desktop reactors using the finite element modelling approach as well as the lumped circuit model.

1.1 Research Question

Reactors are subject to various transients in the power system (switching or lightning). Modelling the frequency response of the reactor would be important to identify any characteristics of interest or design issues that would need to be considered, particularly related to the case where reactors are immersed in a liquid dielectric and significantly cooled.

The research questions are:

- Can the frequency response of the desktop reactor be modelled and analysed by employing FEM methodologies through COMSOL software?
- What factors or parameters in terms of resistance, capacitance and inductance would affect the performance of a fault limiting reactor under transients?
- What models can be used to represent a reactor and can it be extrapolated to represent a full-scale reactor?

1.2 Importance of Study and Contribution

With the demand for electricity continuously increasing, power systems are required to increase capacity to meet such demands which can entail integrating renewable energy resources to the grid and other means of power generation. This increase in capacity would mean a likewise increase in fault levels in the network which can result in costly damage to components such as transformers, generators, switching apparatus and transmission cables.

A local study by Khan et al [1], proposed a superconducting series reactor (SSR) for the management of short circuit currents. This dissertation serves as a contribution towards developing and designing these reactors.

1.2.1 Limitations of the Research

The content of this dissertation is limited to the study of air-core reactors focusing on modelling the frequency response to obtain key factors/parameters that influence a reactor's design and not specifically on the development of the SSR. The models developed are based on standard copper conductors and not on any superconducting material as the complexities around modelling an SSR extends beyond the scope of a Masters dissertation.

1.3 Dissertation Structure

This dissertation consists of seven chapters.

Chapter 1 gives an introduction into air-core reactors and its importance in power networks. This is followed by the research questions and hypothesis for this dissertation, and then the importance of this study and contributions.

Chapter 2 consists of a literature review which delves into the background theory of series reactors, a brief overview of transient over voltages and then research into the electromagnetic behaviour of reactors. The chapter concludes by comparing modelling methodologies found in previous studies and developing a solution for modelling and validating models.

Chapter 3 contains the modelling approaches used (Equivalent Circuit Model and Finite Element Method) as well as the results produced by these models using MATLAB and COMSOL software.

Chapter 4 validates the models developed in Chapter 3 by comparing the models' results to measured values from the desktop reactors.

Chapter 5 documents the sensitivity analysis performed on the COMSOL model for changes to geometry, permittivity of the insulation medium and resistivity of the copper coil

Chapter 6 contains the simulations done for a full scale reactor using the FEM models in COMSOL.

Chapter 7 contains the conclusions found from the simulations as well as further possible steps.

2 Literature Review

This chapter covers an extensive study into the types of reactors commonly used as well as the differences between them and where they may be installed in a network. This continues into the research of the electromagnetic behaviour of these reactors within which, equations for key parameters such as the inductance, capacitance and resistance of reactors are developed for use in the equivalent lumped circuit model in the following chapter. Other important subjects such as the frequency response as well as skin and proximity effects are studied in this section. Different types of modelling methodologies which have been applied in previous studies are investigated and compared to the Finite Element Method.

2.1 Background Theory on Current Limiting Reactors

Current limiting reactors or series reactors are commonly used in power networks to reduce fault currents to levels that the equipment in the network is rated to handle safely. These devices provide an economically viable solution for networks that are continuously increasing generation capacity and installing additional sources of power.

2.1.1 Types of Fault Current Limiting Reactors

The four basic types of current limiting reactors are [2]:

- Air-core reactor
- Oil-immersed gapped iron-cored reactor
- Oil-immersed magnetically-shielded coreless reactor
- Oil-immersed electromagnetically shielded coreless reactor

Two of the most common current limiting reactors employed is the air-core reactor and the iron-core reactor. Air-core reactors may have the issue of stray fields occurring outside the structure but also provide advantages such as a lightweight structure, and can be more cost effective than an iron-core reactor. Air-core reactors also require a larger clearance area to other equipment and objects since the magnetic field extends beyond the physical dimensions of the reactor and its windings as a result of the magnetic field not being constrained by an iron-core. The clearance area required depends on the rating of the reactor, i.e. the higher the rating, the greater the clearance required [3].

Iron-core reactors have a core that is made of a ferromagnetic material which contributes greatly to its overall inductance value. The iron core design is popular due to its ability to contain the magnetic fields within the core thereby preventing stray magnetic fields from occurring outside the structure. The core however, also introduces more losses due to eddy currents and hysteresis.

For magnetically shielded coreless reactors, a magnetic shield is strategically placed around the coils in order to provide a return path for the coil flux which inhibits additional losses to the tank. Similarly, the electromagnetically shielded reactor has shields which are usually made of copper or aluminium situated around the coils to provide a path for the currents to counteract the return flux [2].

2.1.2 Dry-type vs Oil-immersed

The medium within which the reactor's windings operate, can either be a dry-type or oil-type which each has its own advantages and disadvantages depending on the application requirements. With regards to cooling, the dry-type reactor would use the ambient air or require fans and other such means whilst with the oil-immersed windings, the process would involve cooling the oil, similar to that of transformers. However, the dry-type reactor would require far less maintenance than an oil-immersed reactor.

Since oil-immersed reactors usually have an iron-core or have shields in place, the magnetic fields do not stray outside the tank. Hence, these types of reactors would require a smaller clearance area than the dry-type air-core reactors. However, they do introduce an additional capacitance to the reactor which is undesirable and is also why dry-types are commonly used [3].

Trade-offs between the factors mentioned would need to be considered when selecting a reactor for an application.

2.1.3 Structure of an Air-core Reactor

The basic structure of an air-core reactor consists of a winding that can be made of either copper or aluminium which is supported by some structure. This structure is then electrically isolated from the mounting bracket and ground by means of post insulators as shown in Figure 1 [4]. The inductance of air-core reactors is largely determined by the winding itself without any influence from the core.

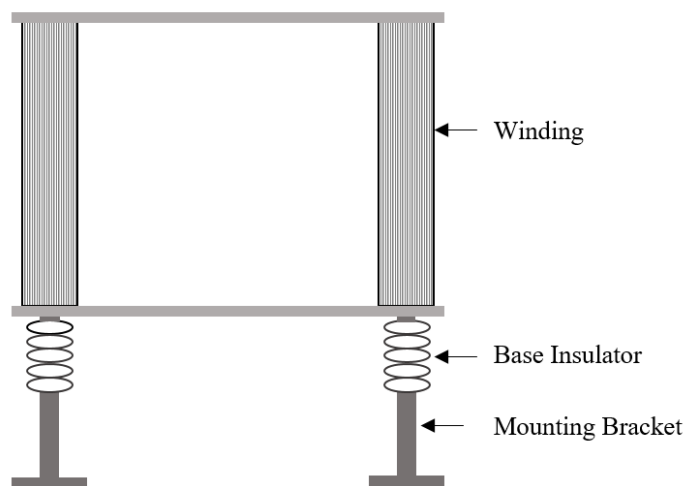


Figure 1: Cross-section of a basic air-core dry-type reactor

2.1.4 Structure of a Coolant Immersed Reactor

Air-core reactors do introduce additional losses to the network during normal operations mainly due to its resistance. Some variations are designed to be immersed in coolants to reduce this resistivity as well as to reduce the heat dissipated during a fault current. The structure here would be similar to that of the dry-type reactor but would also include an appropriate enclosure for the coolant and its maintenance.

2.1.5 Installation Locations of Current Limiting Reactors (CLRs)

CLRs can be classified into three main types based on where they are employed in power networks, namely generator reactors, feeder reactors and bus bar reactors. Each of these reactors come with their own advantages and disadvantages.

2.1.5.1 Generator Reactors

Generator reactors are installed in series to generators in the network as shown in Figure 2. This type of reactor limits the amount of current that would flow into the fault site. The shortcoming of this setup is that synchronism may be lost at the feeders for a three phase generation network, if the fault occurs on one of the feeders. Since the reactors are in series to the generators, they inherently introduce a voltage drop and a power loss to the system.

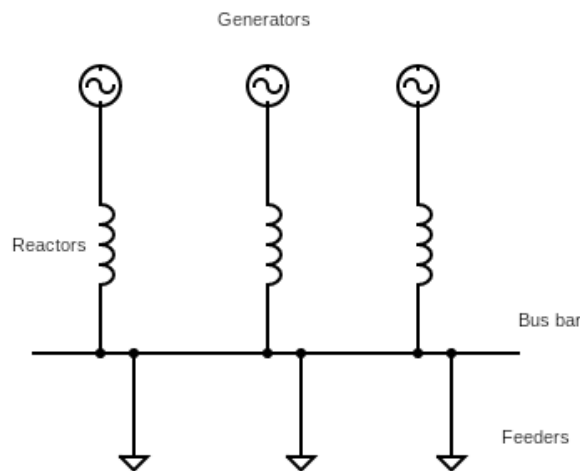


Figure 2: Generator reactors in a network

2.1.5.2 Feeder Reactors

CLRs are installed on the feeders to limit the fault current drawn as shown in Figure 3. The reactor will limit fault currents on a particular feeder, hence it does not protect against bus bar faults. As with the generator reactors, these reactors also have a constant voltage drop across the reactors resulting in a power loss.

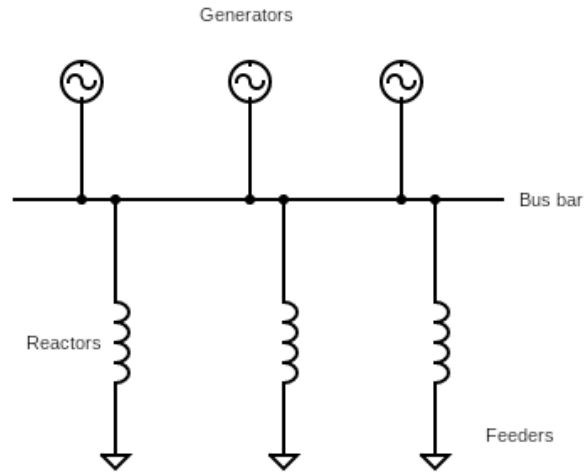


Figure 3: Feeder reactors in a network

2.1.5.3 Bus-bar Reactors

This method of protection has an advantage over the former two in that it reduces the power loss due to the reactors by sectioning the bus bar. This can be done in two ways, the Ring system and the Tie bar system.

The ring system as shown in Figure 4, has the reactors installed on the bus bar between the generators which results in little power flowing through the reactor during normal operations. When a fault occurs on a feeder, the generator connected to it will feed the fault and the other generators will feed it through the reactors [5].

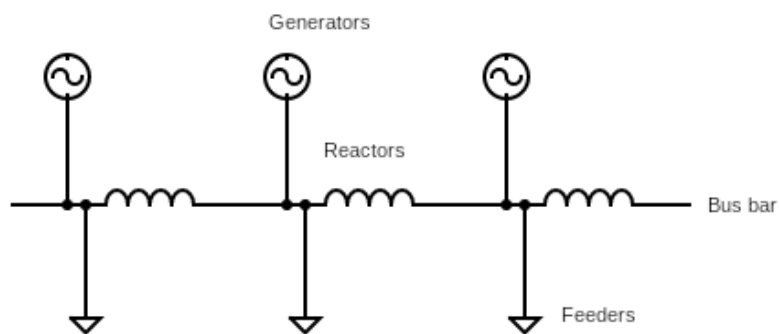


Figure 4: Bus-bar reactors in a network (ring system)

The Tie bar system as shown in Figure 5, offers a more advanced design in that the current fed to a fault would need pass through two reactors in series due to the sectioning.

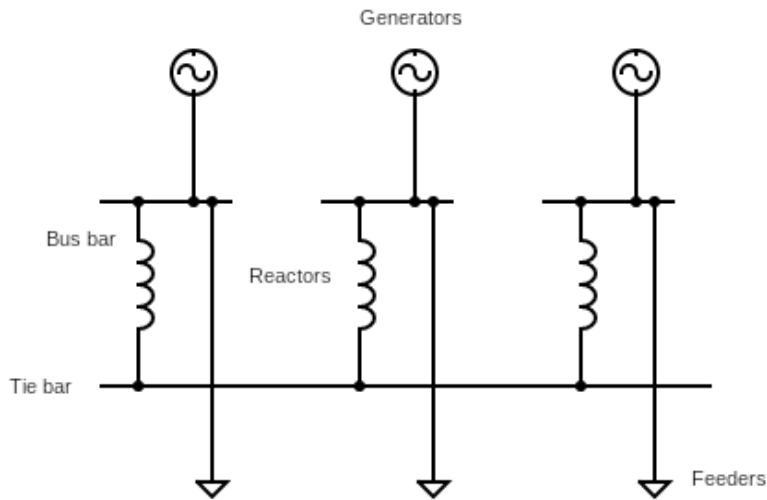


Figure 5: Tie-bar reactors in a network

2.1.6 Other Applications of Air-core Reactors in Power Systems

Aside from fault current limiters, air-core reactors are also used for other applications in power systems. A few common reactors are described in the following sub-sections.

2.1.6.1 Shunt Air-core Reactor

Shunt reactors are commonly used for voltage control or stabilisation, and for the absorption of reactive power in medium voltage distribution systems. Shunt reactors are used to compensate for sudden increases in voltages due to a phenomenon known as the Ferranti Effect. This occurs on long AC transmission lines (long transmission lines have inductive characteristics) when the load on the receiving end of the line is greatly reduced or no longer present which results in voltage at the receiving end being greater than that of the sending end [6]. The shunt reactor at the receiving end would absorb the additional reactive the power and restore voltage stability.

2.1.6.2 Filter Reactor

Also referred to as Harmonic filter reactors are usually connected with capacitor banks and resistors to create filters in order to reduce the harmonic distortion in networks which arise from power electronic equipment and large inductive machines. Harmonic distortions can be quite problematic for networks by introducing greater losses, high neutral currents, interference with computers and other such devices.

2.1.6.3 Neutral Grounding Reactor

Similar to current limiting reactors, this reactor limits current from the neutral point of three-phase systems to ground. In a balanced three-phase system, the reactor will have zero current flow, hence no losses during normal operating conditions.

2.2 Transient Voltages

Transient overvoltages can occur on power supply networks that transmit electricity at high voltages. The occurrence of these overvoltages can be due to direct or indirect lightning strikes, short circuits or flashovers due to electrical insulation breakdown and various switching operations such as the operation of circuit breakers in the network [7].

Temporary overvoltages occur due to events such as earth faults, system faults that lead to switching operations, etc. Slow-front overvoltages generally occur as a result of switching capacitive or inductive currents, fault and fault clearing, line energization, etc.

Fast-front overvoltages occur as a result of lightning strokes and are therefore usually referred to as lightning overvoltages/transients. This transient is characterised by its sharp rise-time (approximately 1.2 μ s to peak) and very high overvoltages that is far greater than other transients.

Very-fast-front overvoltages are more commonly referred to as switching transients and occur due to various switching applications such as the operation of circuit-breakers and transformer tap switching. These transients usually have a rise time to peak of approximately 0.1 μ s or less occur at frequencies ranging between 100 kHz to 50 MHz [4].

These overvoltages can result in large short circuit currents which would need to be reduced by current limiting reactors. The resultant fault currents can be multiple times larger than the operating current which induces electromagnetic forces on the windings of the reactor [5]. The force is a compressive one along the axial length of the winding, which subsequently increases the winding diameter.

2.3 Electromagnetic Behaviour of a Reactor

In order to analyse the electromagnetic behaviour of an air-core reactor, the equations that represent the passive components (capacitive, resistive and inductive) of an air-core reactor must be developed in order to correctly model the reactor and understand its frequency response. Figure 6 shows a circuit representation of an air-core reactor.

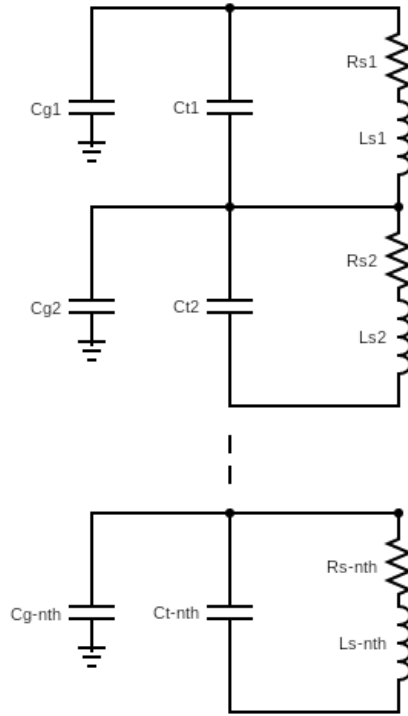


Figure 6: Circuit representation of an air-core reactor coil

R_s , L_s , C_t and C_g represent the series resistance, series inductance, capacitance between turns and ground capacitance of each turn up to the n -th turn,

2.3.1 Capacitive Component

The capacitive component of air-core reactors exists between each individual turn of the winding. The equation used to represent this can be derived from the basic equation for capacitance between two surfaces where an electric field exists,

$$C = \frac{\epsilon_0 \epsilon A}{d}, \quad (1)$$

where A represents the surface area of the winding and d represents the distance between windings as shown in Figure 7. The permittivity of free space and permittivity of the medium separating the two surfaces are represented by ϵ_0 and ϵ respectively.

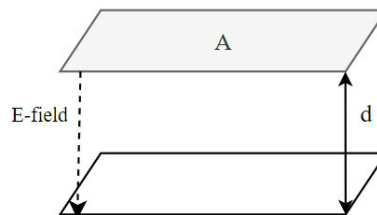


Figure 7: Basic diagram explaining capacitance between planes

Considering the structure of an air-core reactor as shown in Figure 8, the equation for capacitance between two windings is given by [8],

$$C_{t-t} = \frac{\epsilon_0 \epsilon_{air} \pi D_m (w + t_p)}{t_p}, \quad (2)$$

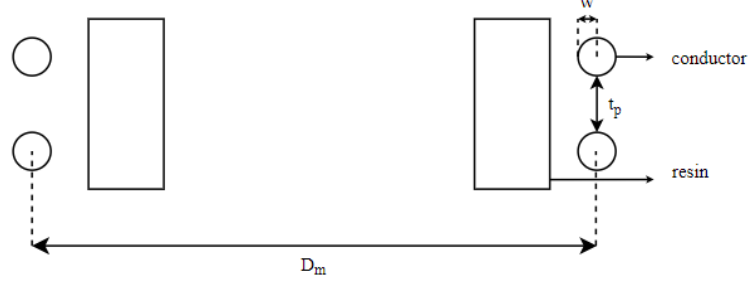


Figure 8: Cross-sectional view of two turns in a reactor

where D_m is the average diameter of the winding, t_p is the distance between turns, w is the radial depth of the conductor and ϵ_{air} is the permittivity of air. In order to account for fringing effects, t_p is added to the width of the conductor [8].

The total series capacitance can then be determined by considering the equation for total energy stored in the windings. The total energy stored in the windings is equal to the sum of all capacitances between turns. This can be represented by equation 3 [8],

$$En = \frac{1}{2} C_{t-t} \left(\frac{V}{N} \right)^2 (N - 1) = \frac{1}{2} C_s V^2, \quad (3)$$

where C_{t-t} represents the capacitance between two windings, N is the number of turns, C_s is the total series capacitance and V is the uniform voltage in the windings. Simplifying this equation, we get the total series capacitance as [8],

$$C_s = \frac{C_{t-t}}{N}, \quad (4)$$

In addition to the capacitance found between turns, a capacitance from each turn to ground is also present. The capacitance between the winding and the tank is determined by [8],

$$C_{gt} = \frac{\epsilon_0 2\pi H}{\cosh^{-1}\left(\frac{S}{R}\right)} \left[\frac{t_{oil} + t_{solid}}{t_{oil}/\epsilon_{oil} + t_{solid}/\epsilon_{solid}} \right], \quad (5)$$

where H is the height of the winding, R is the radius of the winding, s is the distance of the winding to the tank, t_{oil} and t_{solid} is the thickness of the oil and solid insulation present between windings and ϵ_{oil} and ϵ_{solid} is the respective permittivity.

Shortcomings of the above analytical methods are found in its inability to accurately account for stray capacitances. Numerical methods such as the Finite Element Method (FEM) however, does account for stray capacitances which improves the accuracy. In FEM, equation (6) is used to determine the capacitance [8],

$$C = \frac{2En}{V^2}, \quad (6)$$

where En is the total energy stored in the windings and V is voltage across the windings.

2.3.2 Inductive Component

The inductance of a reactor consists of two components, the mutual-inductance and self-inductance and is largely influenced by its physical parameters. Various studies that involve equivalent circuit type models use a matrix approach whereby the mutual and self-inductances of each turn are represented by a matrix.

2.3.2.1 Mutual Inductance

When two coils are in close proximity, the current in the first coil will generate a magnetic field which will interact with the second coil, inducing an emf in the second coil due to the change in magnetic flux. The time rate of change of magnetic flux in the second coil is proportional to the time rate of change of current in the first coil as represented by equation (7), where N_2 is the number of turns in the second coil and M_{21} is the mutual inductance,

$$N_2 \frac{d\Phi_{21}}{dt} = M_{21} \frac{dI_1}{dt}, \quad (7)$$

In the case of an air-core reactor, this inductance is formed between the turns of the winding. The following equation is used to determine the mutual inductance between two coaxial coil loops, X and Y [2]:

$$M_{XY} = \frac{2\mu_0}{k} N_X N_Y \sqrt{R_X R_Y} \left\{ \left[1 - \frac{k^2}{2} \right] K(k) - E(k) \right\}, \quad (8)$$

where

$$k = \sqrt{\frac{4R_X R_Y}{(R_X + R_Y)^2 + S^2}}, \quad (9)$$

R_X and R_Y is the radii of the coaxial coil loops with S being the distance between them as shown in Figure 9:.. N_X and N_Y describes the turns in X and Y respectively and $K(k)$ and $E(k)$ are elliptic integrals of the first and second kinds [2].

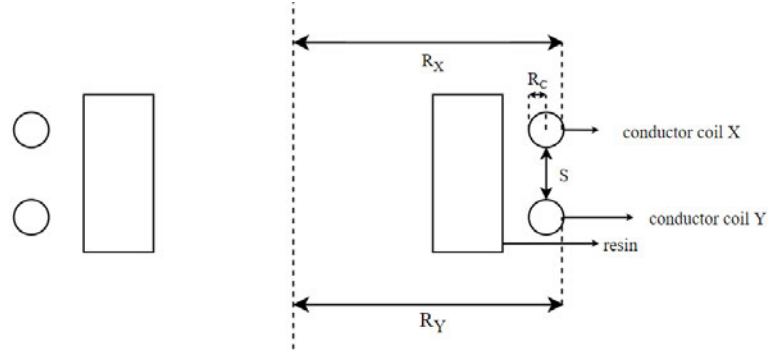


Figure 9: Cross-sectional view of two coaxial coils

2.3.2.2 Self-inductance

Self-inductance refers to the property of a current-carrying loop's magnetic field, opposing any change in current, thereby inducing a back emf.

The equation used to solve for self-inductance is similar to equation (8) for mutual inductance, however the equation for k is solved by incorporating the radius of the conductor (R_C) as shown in equation (10).

$$k_s = \sqrt{\frac{4R_X(R_Y - R_C)}{(R_X + (R_Y - R_C))^2}}, \quad (10)$$

The mutual and self inductances are typically used to form a matrix as shown in equation (11) where the main diagonal of the matrix represents the self-inductances of each turn while the remaining values represent the mutual inductances between respective turns.

$$\begin{bmatrix} L_{11} & L_{12} & \cdots & L_{1m} \\ L_{21} & L_{22} & \cdots & L_{2m} \\ \vdots & \vdots & \ddots & \vdots \\ L_{m1} & L_{m2} & \cdots & L_{mm} \end{bmatrix} \quad (11)$$

2.3.2.3 Inductance of a Solenoid

The total inductance of an air-core reactor can also be determined using Wheeler's formula for a single-layer coil [9].

$$L = \frac{D^2 N^2}{l + 0.45D} (\mu H), \quad (12)$$

where D and l is the diameter and length of the coil respectively in centimetres and N is the number of turns as shown in Figure 10.

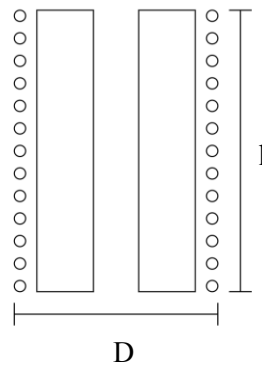


Figure 10: Cross-sectional view of a solenoid

This approach may not be as detailed as the matrix but it does provide an accurate and simplistic approach to estimate the total inductance of an air-core reactor.

2.3.2.4 Looped Inductance vs Partial Inductance

An important concept to consider when calculating inductance is that a complete closed loop must be defined for the current path. This concept is applied for calculating 'looped' inductances since the complete current path is known, however at higher frequencies the complete current path may not be as expected. At higher frequencies, the return path of a current can occur differently, e.g. it may occur on the shielding of a cable resulting in an unexpected current loop [10].

When computing the inductance of a part of a wire loop, we refer to it as partial inductance. Partial inductance allows us to determine the inductance based on physical dimensions of the conductor. The part inductances can then be combined to form the complete overall loop inductance which accounts for partial inductances as well as mutual inductances [10].

2.3.3 Resistance of a Solenoid

In order to determine the resistance of the copper used to construct the reactor coil, the formula for the resistance of a solenoid may be used. Equation (13) is used to determine the length of the copper used,

$$l_c = \pi DN, \quad (13)$$

where D is the mean diameter of a single loop and N is the number of turns. Equation (14) calculates the resistance of the copper,

$$R = \rho \frac{l_c}{A}, \quad (14)$$

where ρ is the resistivity of copper and A is the cross sectional area of the copper wire.

2.3.4 Skin and Proximity Effects

Skin effect is the term given to describe the phenomenon where the current density of a conductor increases towards the surface due to magnetic fields within the conductor responding to high frequency currents. This non-uniform distribution of current within the conductor results in an increase in impedance of the conductor [11]. The formula for skin depth can be represented by,

$$\delta = \sqrt{\frac{1}{4\pi\sigma\mu f}}, \quad (15)$$

where σ , μ and f is the conductivity, permeability and frequency of interest respectively [12].

The resistance as a result of the skin depth is given by equation (16) [13].

$$R_\delta = \frac{1}{\delta\sigma}, \quad (16)$$

Proximity effect describes the further increase in resistance when two conductors carrying high frequency currents are adjacently placed. This occurs as a result of changing magnetic fields having an effect on the current distribution of adjacent conductors [11]. Two adjacent conductors with currents travelling in the same direction would exhibit a lower current density at points that are closest to the adjacent conductor and a higher density at points further away [12].

2.3.5 Frequency Response

Analysing models in the frequency domain are commonly used in many literatures such as [14], [6] and [15] in which a subsequent frequency response would be analysed. The frequency response is essentially a graphical illustration of how a system responds when subjected to different frequencies. A key evaluator is the resonance frequency which is the frequency at which the greatest amplitude would be observed.

For the air-core reactor, the models are solved in the frequency domain in order to find the resonance frequency which is where the maximum impedance of the reactor occurs due to the parasitic

capacitance resonating with the ideal inductance. Moving beyond the resonance frequency, a change from an inductively dominant reactance to a capacitive-dominant reactance should be observed. This can be explained by the equivalent circuit of a coiled inductor shown in Figure 11, where L_c , R_c and C_t represent the coil inductance, resistance and total capacitance respectively [16].

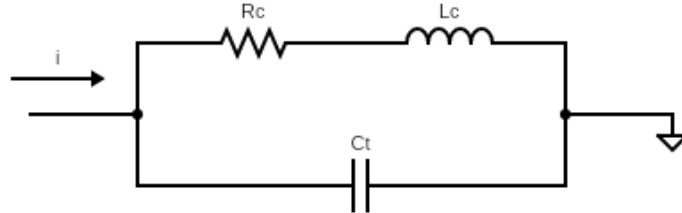


Figure 11: Equivalent lumped circuit of an inductor

As the frequency increases, the impedance of the capacitance decreases and becomes equal to the inductance at resonance, after which the inductor would lose its inductive behaviour [16]. The resonance frequency is required to determine the frequency rating of the reactor as it should not exceed its resonant frequency during fault current limiting.

The resonant frequency, which corresponds to the maximum coil impedance, can be formulaically described as the reactance of the capacitor being equivalent to the inductive reactance. From which, the equation for determining resonant frequency (17) can be obtained [4].

$$\begin{aligned}
 X_L &= X_C \\
 2\pi fL &= \frac{1}{2\pi fC} \\
 f &= \frac{1}{2\pi\sqrt{LC}}, \tag{17}
 \end{aligned}$$

The expected frequency response of a transformer winding is shown in Figure 12 from a case study involving high-frequency modelling of a 500 kV transformer [17]. The shape in Figure 12, which exhibits multiple resonance frequencies, is also seen in a case study done on a 600 MVA single phase transformer where measurements were performed at the terminals of the secondary winding, with the other terminals opened [18]. Note that Figure 12 is a basic replication of the measured frequency response done in [17] with the intention to highlight key points/peaks to expect in a frequency response. A similar frequency response is seen in another study where resonance analysis is done on a transformer winding by Popov [19].

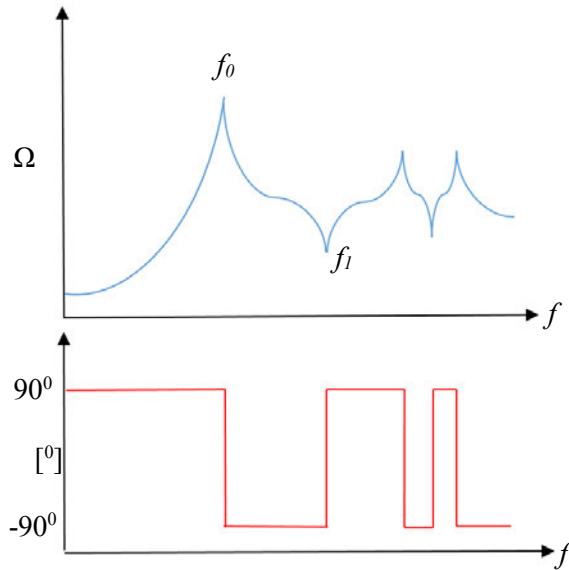


Figure 12: Frequency response of a single phase transformer [17]

The first peak f_0 , refers to the fundamental resonance frequency. The impedance before reaching this frequency indicates an inductive-dominant impedance. Moving beyond this frequency, the impedance exhibits a capacitive-dominant impedance which can be clearly seen with the phase moving from 90° to -90° [18]. The harmonic impedance of the transformer can be clearly seen with the occurrence of multiple resonance peaks [19]. A similar frequency response is expected in an air-core reactor as they essentially have the same coiled structure.

2.4 Modelling Methodologies

A great deal of research has been done into modelling current limiting reactors and as such, various methodologies and approaches to solving problems around current limiting reactors have been developed. The most common of these being the Transmission Line model, the lumped circuit parameter model, the Partial Equivalent Element Circuit (PEEC) method and the Finite Element Method (FEM).

2.4.1 Transmission Line Modelling

Single transmission line (STL) models and Multi transmission line (MTL) models are generally employed for the analysis of fast transients and high frequencies which also describes the characteristics of lightning impulses. Since transformers and reactors share some similarities structurally, modelling methodologies used for transformers can be considered for reactors as well. Each turn in the transformer or reactor is seen as a transmission line and differential equations for the voltage and currents in the frequency domain are developed in terms of key parameters such as resistance, inductance, capacitance and conductance [20].

A report by Banda [21] investigated the resonance behaviour in transformer windings using the Multi-conductor Transmission Line (MTL) model. The MTL model was used to determine the parameters

subsequently determining between which turns the insulation could breakdown, as well as calculating the magnitude of the resonant over-voltages.

In another report [22], Shibuya et al. used the MTL model to determine the high-frequency transients in the winding of the transformer. The MTL model is essentially used to reduce the number of unknown parameters and therefore it is possible to provide voltage and current measurements at any point in the windings. A two-coil model and a full HV winding model for an autotransformer were developed and analysed in this study. The results obtained were compared to results from experiments on an actual two-coil and a full HV winding of a transformer which proved the model's validity.

A combination of STL and MTL was done by Popov et al. [23], in which an algorithm for the computation of very fast transient overvoltages in transformer windings was developed. The STL model is used to determine the voltages of each coil and the results are then used in an MTL model to compute the distributed overvoltages across the entire winding. The model is validated by comparing the results to measurements of a full scale transformer [23].

2.4.2 Lumped Parameter Circuit Model

The lumped parameter circuit approach models a representation of electrical equipment with its respective lumped-elements, i.e. resistance, capacitance and inductance, in order to understand its behaviour under certain conditions [10]. This approach approximates the behaviour of the entire system based on an electrical circuit equivalent. It is important to note that the lumped-circuit approach is valid only if "the largest physical dimension of the circuit is electrically short" [10]. This means the winding's length must be far less than the wavelength. For high frequencies, couplings between all parts of each winding would need to be accounted for by means of a more distributive model.

This approach has been used in various literatures to model equipment such as transformers and reactors. A study by Van Jaarsveld [14] documents the utilisation of the lumped parameter models approach to calculate the inductance, capacitance and resistance of a section of a transformer. The self and mutual inductance values calculated were then exported into an ' $m \times m$ ' matrix where m represents the total number of sections of the transformer being evaluated. A similar approach was used for the capacitance between turns. The analytical equations were then validated with a FEM based software, 'Ansoft Maxwell'. In this study the lumped parameter model is compared to the FEM model and then to measured results as a form of final validation [14].

Hamid et al [24] also incorporated the use of lumped parameters for air core reactors to model its transient response in a 400 kV mechanically switched capacitor with damping network (MSCDN). Parameters were derived based on the physical structure and matrices were developed. These were then evaluated in ATP to show the effects of the reactors parameters.

2.4.3 Partial Element Equivalent Circuit (PEEC)

The Partial Element Equivalent Circuit (PEEC) method models an equivalent circuit representation of a system based on the integral forms of Maxwell's equations. A study by Enohnyaket and Ekman [6] used the PEEC modelling approach for an air-core reactor. This was achieved by representing the individual turns of the reactor by a fixed number of elements, of which equivalent circuit parameters (including partial inductances, coefficients of potential and resistances) were evaluated. These parameters were then evaluated in matrices to solve for the current and voltage distributions. Results were validated by means of measurements of an actual air-core reactor. One advantage of PEEC models is that it can be used in both, the time and frequency domain.

In another study by Kovačević et al [15], the PEEC approach was coupled with the boundary element method to model a 3D toroidal inductor in the frequency domain. The PEEC simulation results were validated by testing and measuring coil impedance. In [25], the PEEC method is coupled with the finite element method (FEM) method to combine the benefits of both methods. The PEEC method would account for the conductors and FEM for the magnetic materials involved in the system.

2.4.4 Finite Element Method (FEM)

The finite element method (FEM) works by splitting structures into several 'elements' and then connects them via nodes. Algebraic equations are developed at these nodes which are then solved [26]. FEM is known for being able to compute across complicated geometries and is used in a variety of engineering problems. For transformers and reactors, FEM can be applied in the analysis of electrostatic and magnetic fields which in turn, helps analyse the frequency response of such systems under transient conditions.

Several studies have been conducted in which parameters of models were determined using the Finite Element Method (FEM). Vahdi et al. [27] simulated transients on cast-resin dry-type transformers using FEM. A 2D axisymmetric model of a transformer was designed in a FEM tool and simulated to obtain the capacitance and inductance parameters. The simulated results were tested against a lab transformer being subjected to impulse tests in order to determine the accuracy and the comparisons showed that this method is suitable for this application.

As stated previously, Van Jaarsveld [14] developed a FEM model in order to validate calculated parameters of an electromagnetic model for a transformer winding. These results were then further validated by comparing them to measured values. A sensitivity analysis of the mesh used in the simulation of the FEM was conducted to ensure accuracy of the model. When using FEM methodologies, conducting a sensitivity analysis of the mesh is imperative to ensure the accuracy of the model. Meshing is the division of geometry into smaller elements and the basic rule is the finer the mesh, the more accurate the results. However, the finer the mesh used, the more computationally

expensive is the simulation. Hence, it is project dependant on how fine a mesh needs to be for the model to be considered accurate [8].

FEM based software such as FEMM and Ansys provide researchers with simpler options to compute certain parameters such as capacitances and analyse the behaviour of transformers and similar devices effectively as seen in papers [28], [29] and [30].

2.4.5 Summary of Modelling Methodologies

The methodologies in the previous sections have all proven to be successful and show various advantages and complexities in their respective implementations. Software applications can assist in simplifying the simulation process and obtain accurate results efficiently. Whilst most of the modelling approaches require analytic computations to obtain parameters, FEM has various software applications based on its methods to automatically solve and determine these parameters. For solving analytic computations, programs such as MATLAB can be used with Simulink or SPICE for circuit simulations. Ansys, COMSOL Multiphysics and FEMM are popular simulation software that's based on FEM methodologies, which simplify the implementation making rescaling and simulations more efficient. COMSOL has been used in several papers such as [31] and [32] for various problems and has been proven to be both versatile and powerful. COMSOL also allows for the development and analysis of frequency responses of complex geometries while taking into account materials and physics making it ideal for air-core reactors.

Based on the research conducted in the preceding sections, it was decided that the approach for this dissertation is to develop a FEM model for a desktop air-core reactor using COMSOL Multiphysics software as well as an equivalent circuit model to assist and guide the development of the FEM model. The FEM model is then compared to measured results of a desktop reactor as a form of final validation of the model before scaling the model for a full scale air-core reactor.

3 Reactor Models

This section covers the development of the Equivalent Circuit Method (ECM) and Finite Element Method (FEM) models for two desktop air-core reactors using MATLAB R2020a and COMSOL Multiphysics software. The corresponding frequency responses and parameter values for resistance, capacitance and inductance are obtained through computations and simulations. The models were developed according to the specifications of the desktop air-core reactors as shown in Table 1. Note Reactor 2 does not have the copper side-plates on the resin core like Reactor 1.

Table 1: Dimensions of the desktop reactor

Parameter	Reactor 1	Reactor 2
No. of turns	17	100
Resin: Inner diameter	30 mm	180 mm
Resin: Outer diameter	55 mm	174 mm
Resin: Height	100 mm	170 mm
Conductor diameter	3.15 mm	1 mm
Copper plates height	7 mm	

Figures 13 and 14 show the desktop reactors used for modelling and validation.

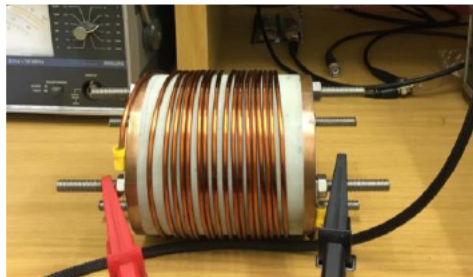


Figure 13: Desktop Reactor 1



Figure 14: Desktop Reactor 2

3.1 Equivalent Circuit Model

The resistance, inductance, capacitance and expected resonant frequency values for the windings of the air-core reactors were computed using the analytical equations from Section 2.3, in MATLAB R2020a. These parameters are computed to guide and validate the development of the Finite Element Method model and verified by measurements in Chapter 4.

3.1.1 Inductance Calculations

Since the aim of calculating the inductance was to obtain a total inductance for the device for guiding the development of the FEM model, Wheeler's formula (12) was used to determine a total inductance of the reactors as shown in Table 2.

Table 2: Calculated Inductance values for Reactor 1 and 2

Inductance Parameter	Reactor 1 (μH)	Reactor 2 (mH)
L_{coil}	23.391	1.3

3.1.2 Capacitance Calculations

The capacitance between two turns (C_{t-t}) of the winding was determined using equation (2) which, subsequently used in equation (4), solved for the total series capacitance of the coil (C_s). Capacitance of the core (C_{core}) can be easily determined with the basic equation for capacitance, i.e. equation (1), which is an additional parallel capacitance in circuit terms. The results obtained from these calculations are tabulated in Table 3. The approximate total capacitance (C_{tot}) is the sum of the series capacitance (C_s) and ground capacitance (C_{g-t}).

Table 3: Capacitance values computed using MATLAB

Capacitance parameter	Reactor 1 (pF)	Reactor 2 (pF)
C_{t-t}	39.341	142.13
C_s	2.3142	1.4213
C_{core}	2.9541	0.43422
C_{g-t}	1.0285	1.8008
C_{tot}	6.2968	3.6563

3.1.3 Resistance Calculations

The resistance of the coils for the reactors were determined by using the equation for resistance of a solenoid, i.e. equation (14). The corresponding values of resistance are tabulated in Table 4.

Table 4: Calculated resistance values for Reactor 1 and 2

Resistance Parameter	Reactor 1 (Ω)	Reactor 2 (Ω)
R_{coil}	0.613m	0.3101

3.1.4 Resonance Frequency Calculations

The resonance frequency of the two reactors were then calculated using equation (17) and the results tabulated in Table 5. These values guided the modelling process by providing an estimated resonant frequency to expect during simulations.

Table 5: Calculated resonance frequencies

Parameter	Reactor 1 (MHz)	Reactor 2 (MHz)
f_{res}	13.04	2.32

3.2 Finite Element Model

Two FEM models were developed using COMSOL Multiphysics based on the two reactors previously mentioned and the results are then analysed. The model for Reactor 1 is used to explain the development process in COMSOL in terms of geometry, materials used and physics applied.

3.2.1 Geometry

The air-core reactor was developed in a 2D-axisymmetrical plane as shown in Figure 15 with dimensions corresponding to the test reactor. The dimensions used to construct the geometry in COMSOL are tabulated in Table 1. Figure 16 shows the revolution of the 2D-axisymmetric model.

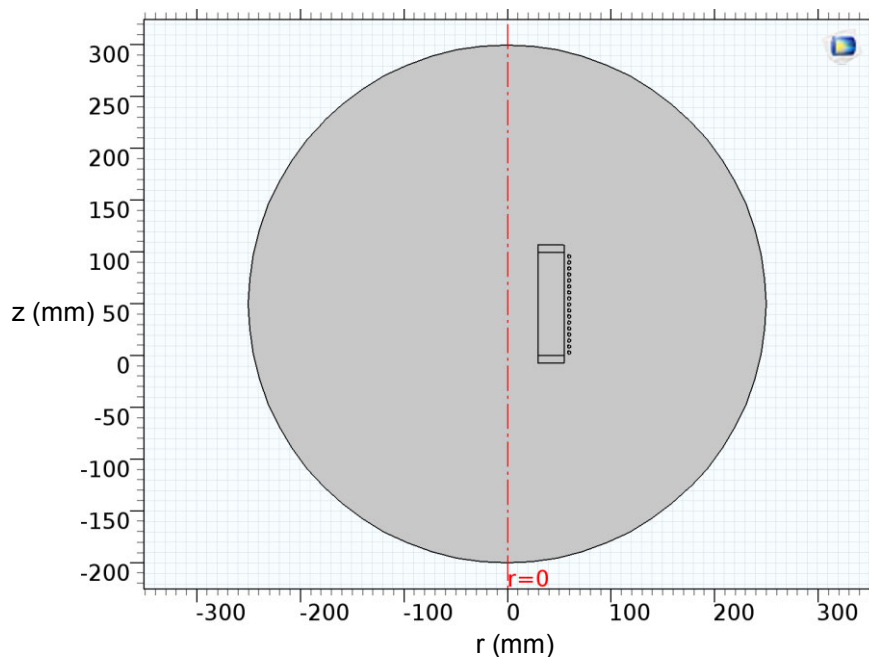


Figure 15: Full geometrical structure representing Air-core reactor in 2d-axisymmetrical plain

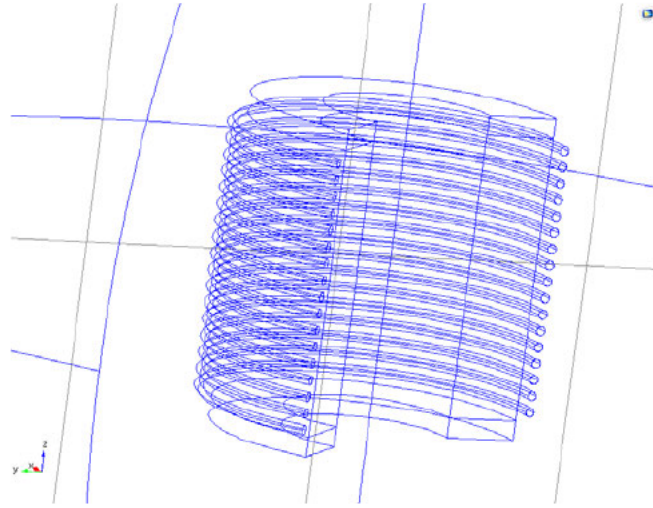


Figure 16: 3D visual of constructed Air-core reactor model

3.2.2 Materials

The materials and properties of materials used are tabulated in Table 6.

Table 6: Table of material properties for FEM model

Material	Relative permittivity	Relative permeability	Electrical conductivity (S/m)
Copper	1	1	5.988e7
G10-resin (Reactor 1)	4.8	1	1.019e-12
Resin (Reactor 2)	5	1	1.019e-12
Air	1	1	0
Nitrogen (liquid)	1.45	1	0

Figure 17 shows which geometrical components utilise the materials from Table 6.

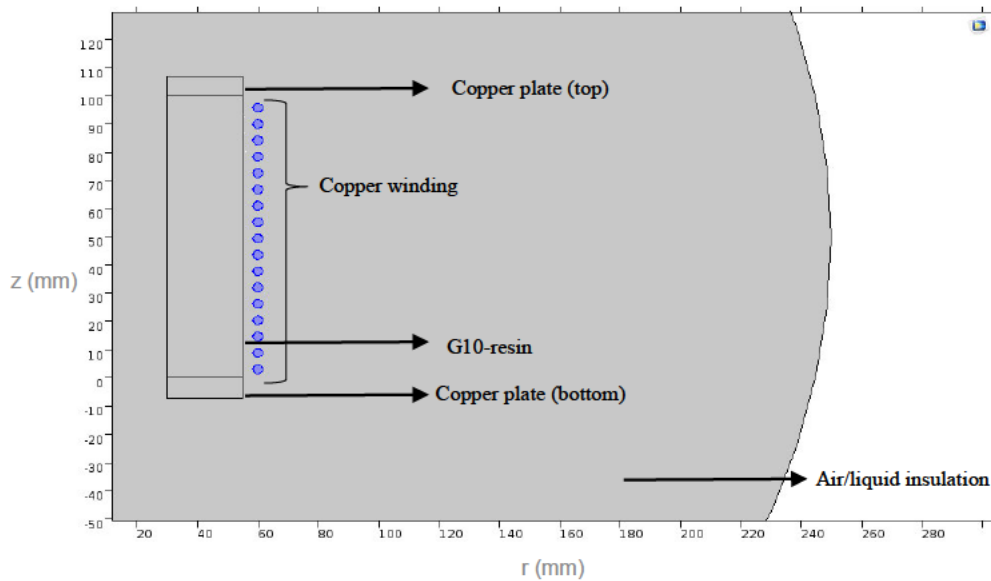


Figure 17: Components of structure labelled with corresponding materials

3.2.3 Physics

The Magnetic and Electric Fields (MEF) physics interface from the AC/DC module was applied to the geometry and is governed by the Ampere's Law and Current Conservation feature. This physics interface solves Maxwell's equations incorporating vector magnetic potential (\mathbf{A}) and scalar electric potential hence its ability to compute magnetic fields and current distributions [33]

Equations (18), (19), (20), (21) and (22) are employed by MEF physics to solve problems in the frequency domain and represent respectively the equation of continuity for electric currents, Ampere's law in point form, the vector magnetic potential, the electric field and current density,

$$\nabla \cdot \mathbf{J} = 0, \quad (18)$$

$$\nabla \times \mathbf{H} = \mathbf{J}, \quad (19)$$

$$\mathbf{B} = \nabla \times \mathbf{A}, \quad (20)$$

$$\mathbf{E} = -\nabla V - j\omega \mathbf{A}, \quad (21)$$

$$\mathbf{J} = \sigma \mathbf{E} + j\omega \mathbf{D}, \quad (22)$$

MEF physics also provides the feature of RLC coil groups which allows for the capability of modelling a copper wire as an RLC coil by applying this feature to the appropriate domains of the geometry as shown in Figure 18. These domains are also automatically governed by Ampere's Law. Hence, equations (17), (19), (20) and (21) also govern the cross sections of the coils with equation (21) being modified to equation (23) since the electric potential is assumed to be constant and electric fields need to be mitigated for each of these cross sections [33],

$$\mathbf{E} = -j\omega \mathbf{A}, \quad (23)$$

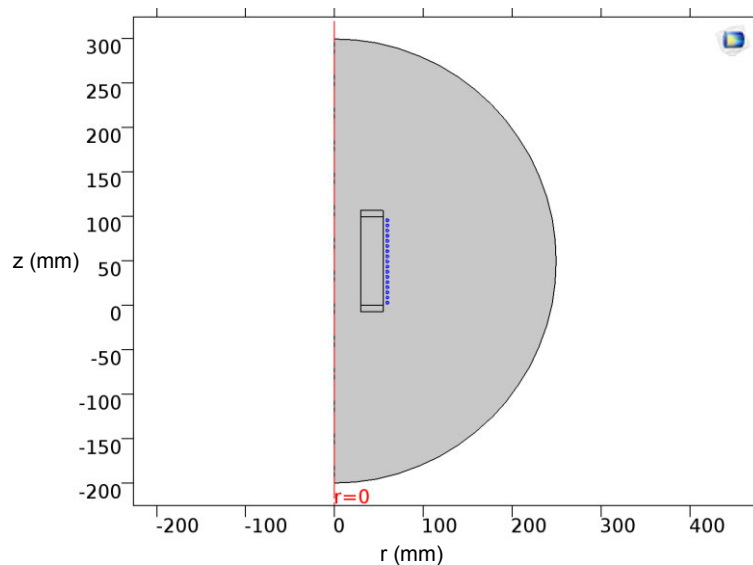


Figure 18: RLC coil group highlighted in blue governed by Ampere's law

The wire domains of the air-core reactor were configured as part of an RLC coil group with a coil current of 1 A and ground voltage of the winding set to 0 V. Current leakage and current flow are also controlled by the physics.

The magnetic and electric fields interface provides the default magnetic boundary condition called ‘Magnetic Insulation’ which also includes ‘Electric Insulation’, the electric boundary condition. As described in the COMSOL Multiphysics documentation [33], the Magnetic Insulation node sets the components of magnetic potential which are tangential, to zero on the boundary of which it is applied, i.e. $\mathbf{n} \times \mathbf{A} = 0$. Electric Insulation, the subnode of Magnetic Insulation, is included by default to ascertain that both magnetic and electric potentials are accounted for. The outer most boundary as shown in Figure 19, is grounded by adding a ‘ground’ to the Magnetic Insulation subnode. This boundary is intentionally constructed at a large distance from the geometry of the reactor itself so as to minimise the capacitive effect as the focus of the simulation is mainly on the frequency response of the RLC components of the reactor itself.

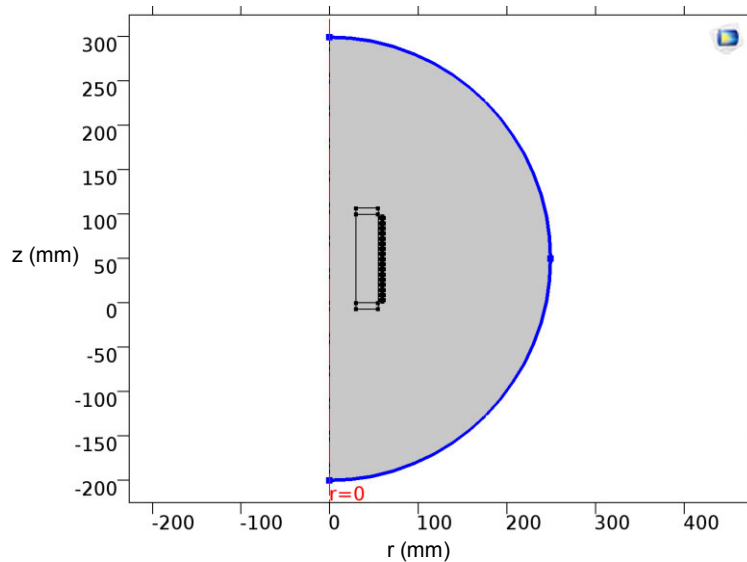


Figure 19: Magnetic insulation boundary

3.2.4 Mesh Settings

The default mesh settings provided, range from extremely-coarse to extremely-fine and can be user modified. The default physics-controlled meshing allows the software to automatically generate an optimal mesh sequence. For the simulation of the air-core reactor, a physics-controlled mesh is used but a sensitivity analysis is still conducted to ensure results are accurate and to identify what parameters are affected by the meshing.

3.2.4.1 Mesh Sensitivity

As mentioned in previous sections, when modelling with the FEM approach, a mesh sensitivity analysis is imperative to ensure accuracy of the model being developed. It is also important to identify which parameters of the air-core reactor are affected by the mesh and to what extent are they affected.

Table 7 shows a summary of how Reactor 1's RLC parameters are affected by four different mesh settings.

Table 7: Mesh sensitivity analysis at 1kHz for Reactor 1

COMSOL Mesh setting	Inductance (μH)	Resistance ($\text{m}\Omega$)	Capacitance (pF)
Extremely-fine	20.784	0.19302	8.1784
Extra-fine	21.086	0.19510	8.2457
Normal	21.087	0.19519	7.9425
Extra-coarse	21.020	0.20315	3.9944

It can be seen that the capacitance is greatly affected by the size of the meshing used while the difference in inductance and resistance can be considered negligible. A 3.8% change in the capacitance can be seen between a 'normal' and 'extra-fine' mesh while the difference between 'normal' and 'extra-coarse' changes the capacitance by 49.7% indicating an anomaly. The extra-coarse mesh setting would not be able to accurately represent a coiled geometry due to there being far too few elements. The vertices and edges that make up the elements are too large to clearly represent a curved geometry therefore it is expected that the extra-coarse mesh setting would not provide accurate or valid results. Appendices A1 to A4 contain images of Reactor 1 from COMSOL to further substantiate this.

Figure 20 compares the effects the different mesh settings has on the frequency response for Reactor 1. Most notably, the 'extra-coarse' is an outlier with an exaggerated impedance but shows a resonance frequency occurring at the same point as the 'normal' and 'extra-fine' mesh. The accuracy of the results obtained has a direct proportionality to how fine a mesh is used. This is expected since the number of elements that describes the geometry increases with a finer mesh.

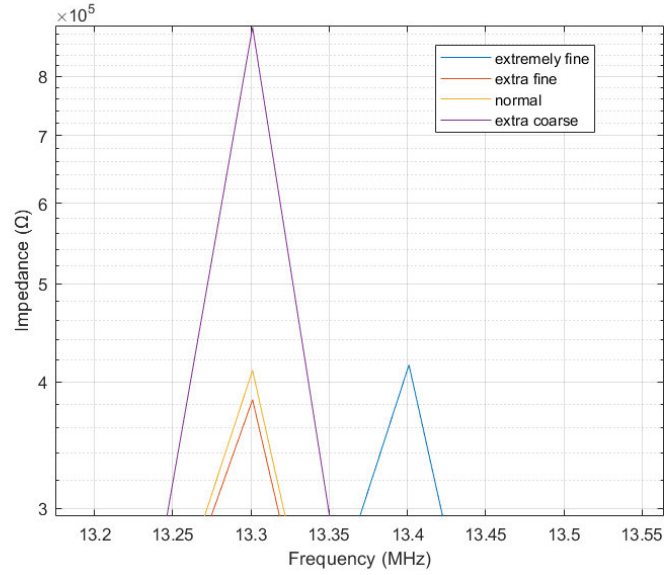


Figure 20: Mesh setting effects on resonance frequency

Since mesh settings has an immense effect on the accuracy of the capacitance, an ‘extra-fine’ mesh setting would be sufficient to produce an accurate model. The difference between ‘extra-fine’ and ‘extremely-fine’ is minimal and should be used if computation time is of no concern and if the device running the simulation permits the memory intensive task. Note that these factors would increase as the size of the model increases as well. For the simulations done in this dissertation, an ‘extremely-fine’ mesh setting was used in order to validate the model.

3.2.5 FEM Results Reactor 1

The model was solved using the ‘frequency domain’ study with the frequency ranging between 1 kHz to 60 MHz in steps of 100 kHz. A coil excitation current of 1 A is applied to the RLC coil group. This study was chosen in order to compute the frequency response of the model. The resonance frequency occurs at 13.4 MHz as shown in Figure 21 and the corresponding phase angle changes can be seen in Figure 22 which shows the change from inductive dominance to a capacitive dominance when going beyond the resonance frequency.

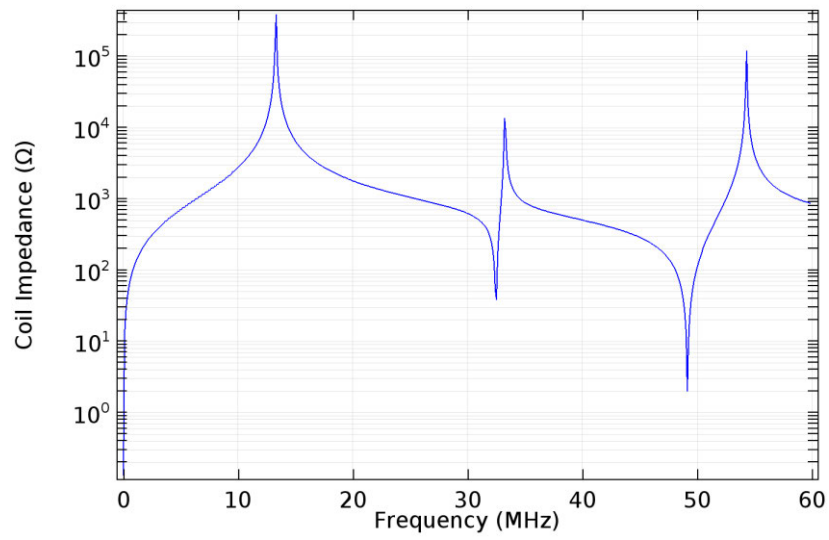


Figure 21: Frequency response of COMSOL model showing Impedance vs Frequency for Reactor 1

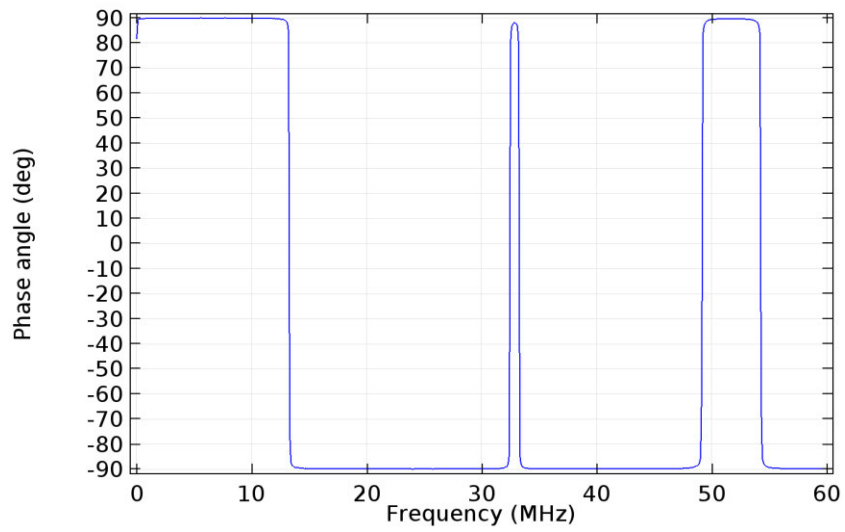


Figure 22: Corresponding Phase vs Frequency for COMSOL model for Reactor 1

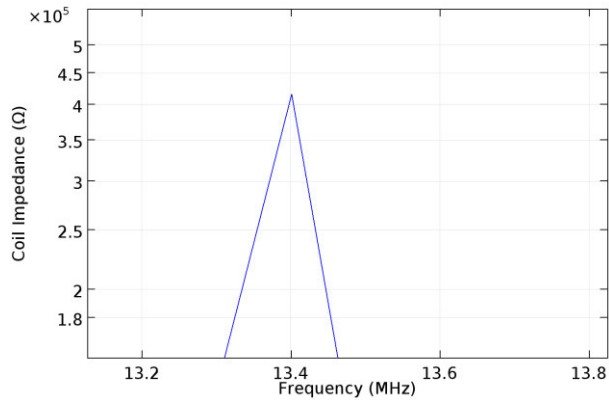


Figure 23: Zoomed resonance peak for Reactor 1 frequency response

The resonance frequency of 13.4 MHz is in strong agreement with the calculated resonant frequency obtained from the ECM model of 13.04 MHz. The peaks seen in the frequency response strongly correlate to the expected frequency response shape as seen in Figure 12. The harmonic impedance with multiple resonance frequencies can be seen which is in agreement of what was expected in terms of the fundamental frequency response followed by the additional resonant peaks as seen in previous literatures [17] [19].

Table 8 shows the parameters at 1 kHz obtained from COMSOL and the corresponding electric field and electric potential at this point are respectively shown in Figure 24 and 25.

Table 8: Reactor parameters at 1kHz for Reactor 1

Parameter	Value
Inductance	20.784 μH
Capacitance	8.1784 pF
Resistance	0.1930 m Ω

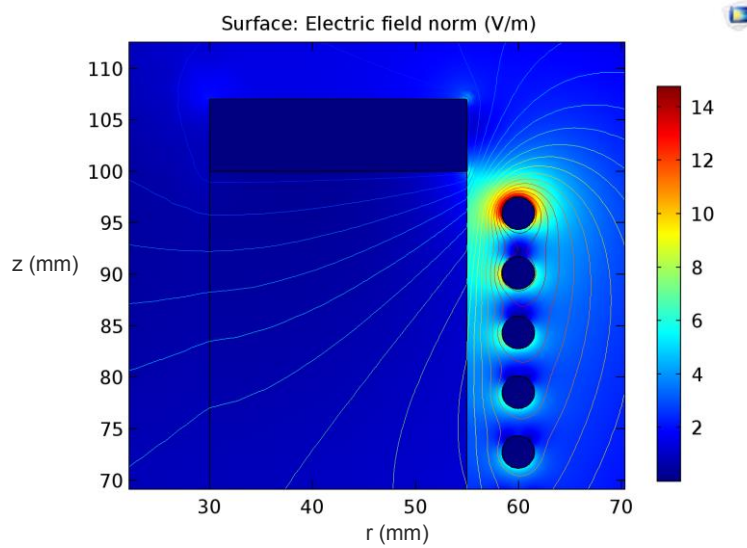


Figure 24: Electric field at 1kHz for Reactor 1

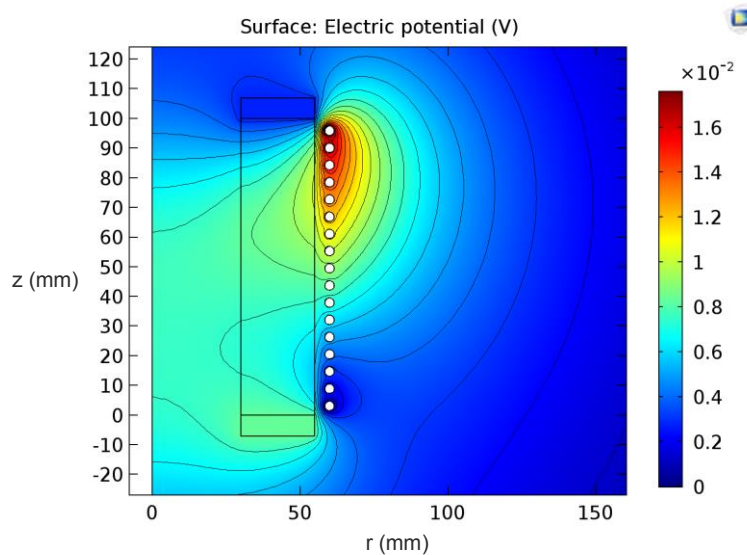


Figure 25: Electric potential at 1kHz for Reactor 1

3.2.6 FEM Results Reactor 2

As done in subsection 3.2.5 for Reactor 1, a COMSOL model is also developed for Reactor 2 and the respective frequency response and phase of the reactor in the frequency range of 0 kHz to 20 MHz obtained can be seen in Figures 26 and 27. A coil excitation current of 1 A is also applied to the RLC coil group. The resonance frequency is observed at 1.5 MHz in Figures 26 and 28 with the expected change in phase angle as seen in Figure 27 indicating a change from inductive to capacitive dominant impedance.

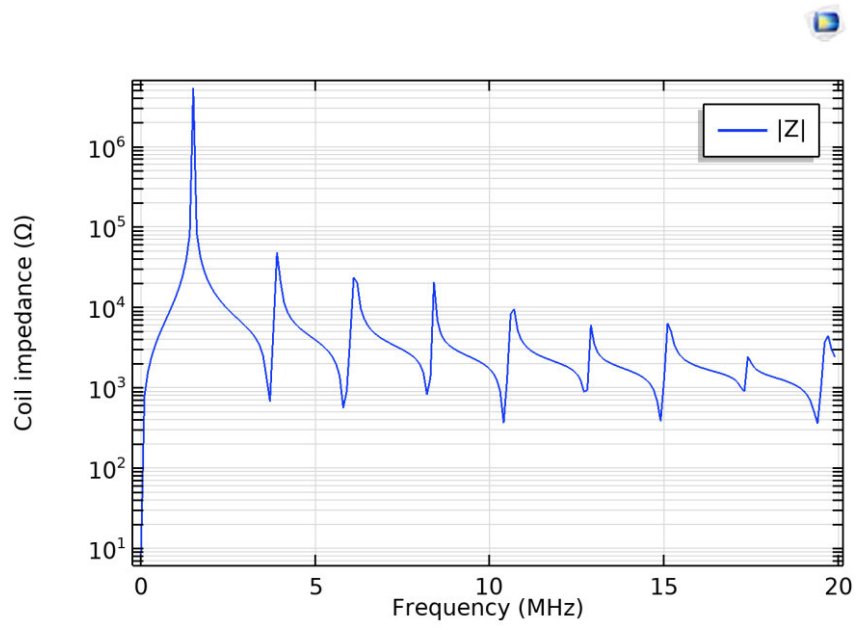


Figure 26: Frequency response of COMSOL model showing Impedance vs Frequency for Reactor 2

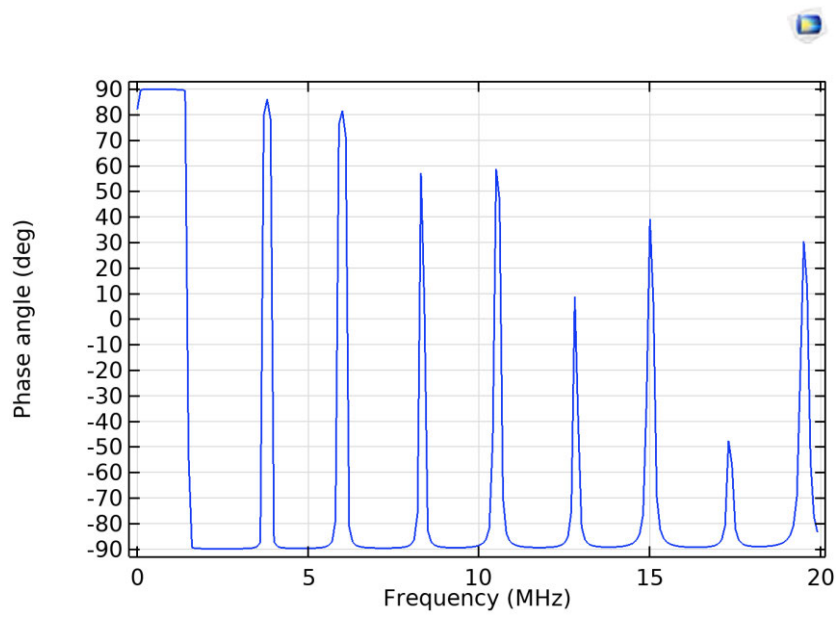


Figure 27: Corresponding Phase vs Frequency for COMSOL model for Reactor 2

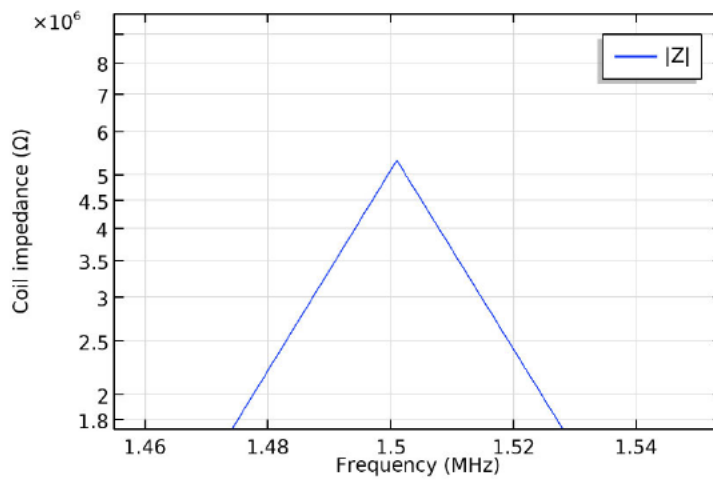


Figure 28: Zoomed resonance peak for Reactor 2 frequency response

For Reactor 2, the frequency response is in strong agreement with what was expected in terms of a fundamental frequency response followed by multiple resonance peaks. The harmonic impedance nature is clearly seen as well with more resonant peaks. Figures 29 and 30 show the respective electric field and electric potential where a more even distribution can be seen compared to Reactor 1 due to the exclusion of copper plates

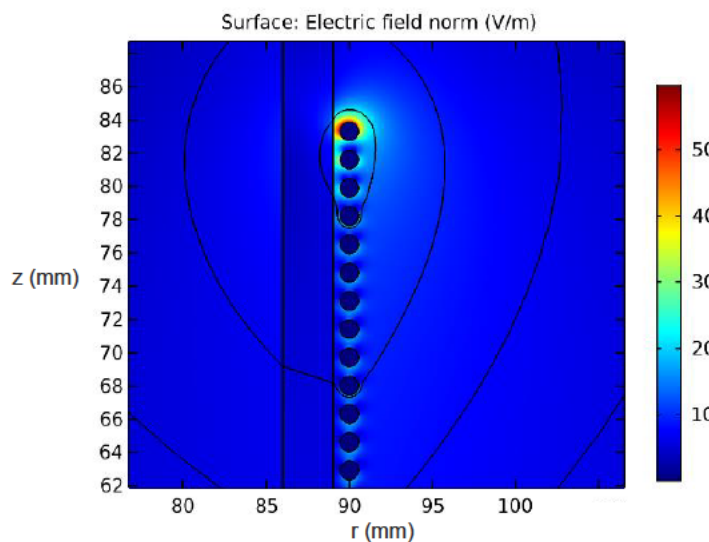


Figure 29: Electric field at 1kHz for Reactor 2

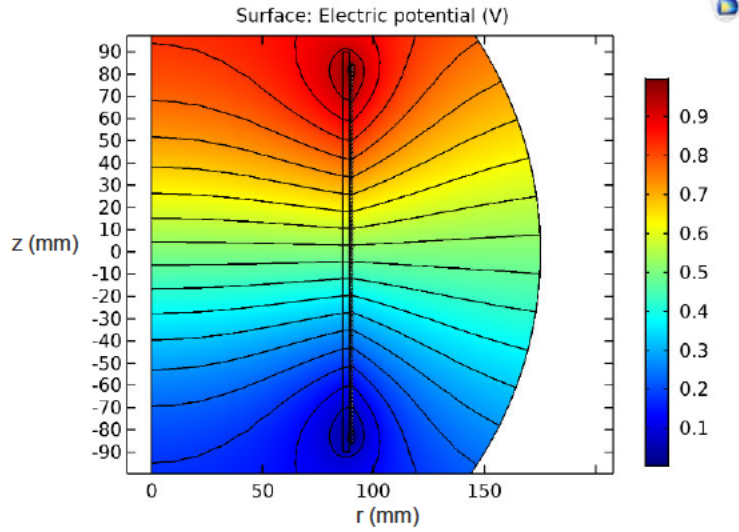


Figure 30: Electric potential at 1kHz for Reactor 2

The RLC parameters obtained from COMSOL are shown in Table 9 and are also in strong agreement with what was calculated in Section 3.1.

Table 9: Reactor parameters at 1 kHz for Reactor 2

Parameter	Value
Inductance	1.2180 mH
Capacitance	4.5813 pF
Resistance	1.0650 Ω

4 Measurements of Reactor

This Chapter aims to confirm if the reactors can be accurately modelled in COMSOL through the comparison of parameters measured and frequency responses recorded. In order to validate the models, measurements of Reactor 1 parameters were recorded at a frequency of 1 kHz and compared to the parameters obtained by the ECM and FEM model. The process for obtaining the frequency response of Reactor 2 is documented and the results compared to simulated results for validation of the models.

4.1 Reactor 1 Measurements

Measurements for Reactor 1 were done using an LCR meter with the aim of recording parameter values to compare the simulated and calculated parameters.

4.1.1 Laboratory Setup

The values of inductance, capacitance and resistance were recorded using an LCR meter (Fluke PM6303A) as shown in Figure 31. An LCR meter is a digital measurement instrument used to record such parameters by sending a signal at specific frequencies to the device being tested.

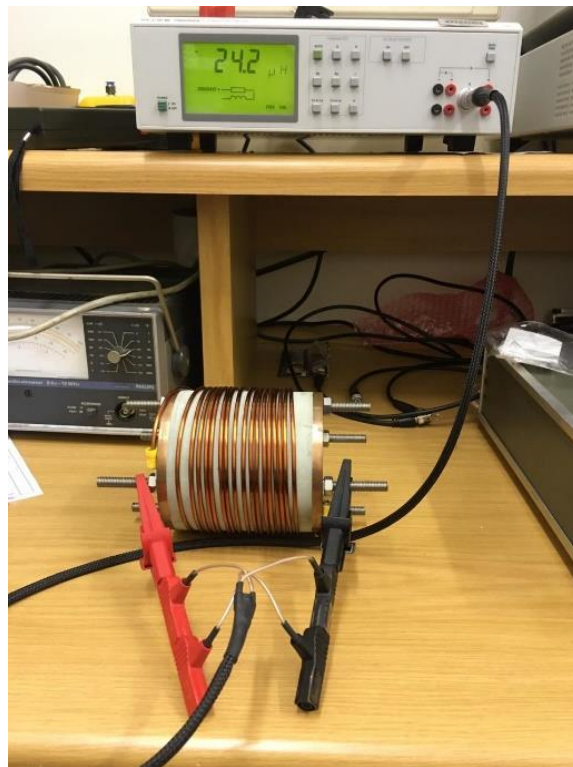


Figure 31: Inductance measurement of the desktop reactor

4.1.2 Measured Quantities

The measurements recorded in Table 10 were taken at a frequency of 1 kHz. Appendices B1 to B4 contains the images of the laboratory setup and measurements taken for desktop reactor 1.

Table 10: Table of recorded parameters for desktop reactor 1

Measurement	Measurement value
Inductance	24.2 μH
Capacitance of reactor	7.2 pF
Capacitance of cable	60.8 pF
Total Capacitance	68 pF
Resistance	0.17 Ω
Phase angle (between and R and I)	41.6 $^\circ$

4.2 Reactor 2 Measurements

Measurements for Reactor 2 were done with the aim of obtaining a frequency response to compare to the simulated frequency response.

4.2.1 Measurement System for the Impedance Measurement

Figure 32 shows the circuit representation for the measurement system that was setup to measure the impedance of the reactor in order to obtain its corresponding resonant frequency. The circuit representation shows the impedance of the measurement cables used as well as the reactor or DUT (Device Under Test).

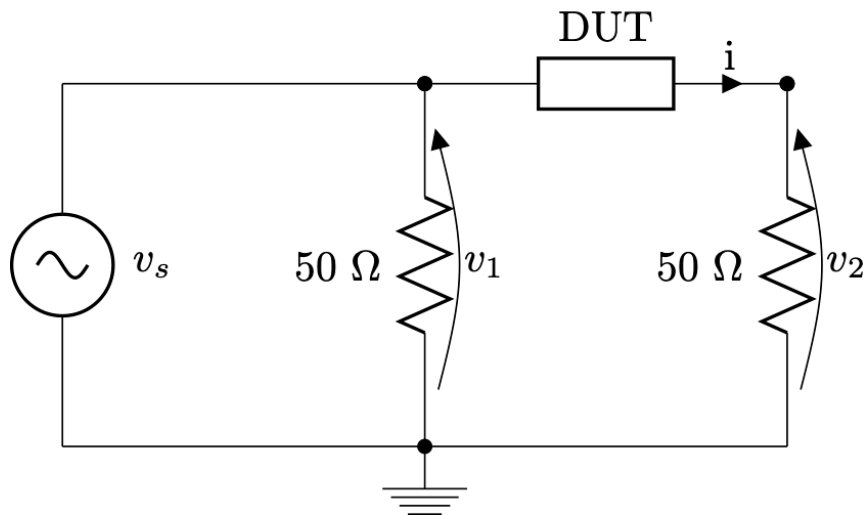


Figure 32: Measurement system for impedance measurement

4.2.2 Device Description

The task of measuring the frequency response of the DUT would require a device capable of calibration to mitigate the effects of the impedance of the measurement leads whilst also being able to provide accurate results for high frequency ranges.

Some devices allow for communication through Standard Commands for Programmable Instrumentation (SCPI) commands. This provides an added advantage in that the device can be remotely controlled through some additional software such as MATLAB or LabVIEW. SCPI commands allows a user to quickly and effectively generate signals and obtain data on measurements from tests performed. Three devices were used in the experiments for measuring the frequency response of the DUT for this setup.

4.2.2.1 Red Pitaya

The Red Pitaya (Figure 33) is a versatile device that can be calibrated and has several applications that allows it to work as a bode analyser, vector network analyser, function generator and an oscilloscope. The bode analyser would be used for frequency response analysis and the function generator and oscilloscope application would be used as well for creating input signals. The Red Pitaya also has the capability of being controlled remotely using Red Pitaya SCPI commands implemented through MATLAB, LabVIEW, Scilab or Python.



Figure 33: Red Pitaya device

4.2.2.2 Picoscope

The Picoscope which is essentially an oscilloscope, is used in applications involving power electronics, signal processing, embedded systems, etc. The Picoscope also has a built-in arbitrary waveform and function generator. For this test, the Picoscope was used in conjunction with an application (FRA4PicoScope) developed by Hexamer which allows for frequency response analysis with Picoscope instruments.

4.2.2.3 GW Instek AFG

The Arbitrary Function Generator (AFG) as shown in Figure 34 is used in conjunction with a toolbox from MATLAB for instrumentation control since the AFG can communicate with SCPI commands. The AFG can produce signals of various shapes at high enough frequencies and voltages to make it a viable device for our test purposes.



Figure 34: GW Instek AFG

MATLAB’s instrument control toolbox allows one to control devices such as oscilloscopes, function generators and analytical instruments. Data or commands can be generated in MATLAB and sent to devices for various purposes such as signal generation, and results can be read back into MATLAB for analysis.

4.2.3 Device Specifications

Table 11 provides detailed specifications for the devices used in the experimental process of measuring the frequency response of the reactor.

Table 11: Detailed specifications of measurement devices

Parameter	Red Pitaya STEMLab 125-14	Picoscope 6406D	GW Instek AFG-2225
Input Voltage	2 V _{pp} on LV Setting 40 V _{pp} on HV Setting	50 mV to 5 V	
Input Voltage Resolution	1.22 mV	50 mV	
Input Sample Rate	125 MS/s	5 GS/s	
Input Bandwidth	60 MHz	25 MHz	
Input Impedance	1 MOhm / 10 pF	1 MOhm / 50 Ohm	
Output Voltage	2 V _{pp}	4 V _{pp}	10 V _{pp}
Output Sample Rate	125 MS/s	200 MS/s	120 MS/s
Output Bandwidth	60 MHz	20 MHz	25 MHz
Output Impedance	External 50 Ohm BNC	Internal 50 Ohm	Internal 50 Ohm

4.2.4 Results

Impedance measurements of Reactor 2 were conducted using the above mentioned devices and techniques in order to validate the models. The results of these experiments can be seen in Figure 35 with Table 12 describing the legend.

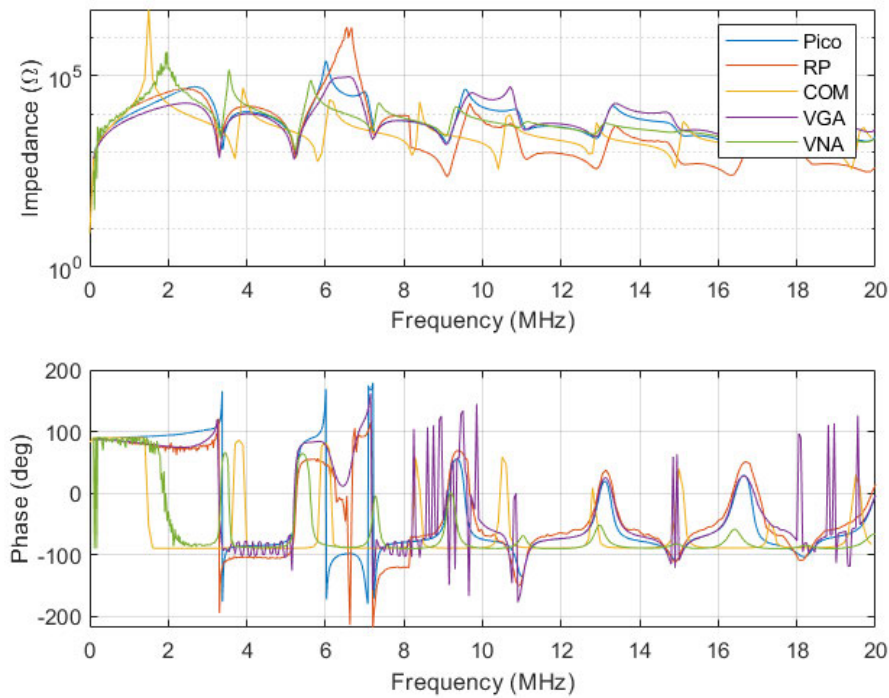


Figure 35: Comparison of frequency responses for Reactor 2

Table 12: Legend description

Legend	Description
Pico	Picoscope
RP	Red Pitaya Bode Analyser
COM	Comsol model (FEM simulation)
VGA	Red Pitaya + AFG
VNA	Red Pitaya + Vector Network Analyser

The sections below describe the experimental process followed for all four setups and provides a detailed explanation of the results seen in Figure 35.

4.2.4.1 Experiment 1: Red Pitaya Bode Analyser

The first experimental setup attempted to measure the impedance of the coil by utilising two applications available on the Red Pitaya device, i.e. Digital oscilloscope and function generator, and

the Bode analyser application. The initial application generates the input signal to the reactor and the latter would measure the response of the reactor. The Bode analyser allowed for calibration which mitigates impedance effects of the measurement leads.



Figure 36: Experiment 1 setup using Red Pitaya

The results yielded were unsatisfactory as it resulted in a frequency response with no distinct peaks. The issue here was that the output of the function generator was limited to $2 V_{pp}$ which means that when the impedance of the coil is very high (at resonance), the current through the impedance is very small, or below the range.

4.2.4.2 Experiment 2: Picoscope

The second experimental setup sought to improve on the indistinct peaks by increasing the voltage level of the input signal. The Picoscope generated a test signal and the results were obtained and analysed through the FRA4Picoscope tool. However, despite an increase to $4 V_{pp}$, the improvement to the frequency response was minimal. The FRA4Picoscope tool does not allow for calibration which was another concern here since these measurements are done at high frequencies.

4.2.4.3 Experiment 3: Red Pitaya and AFG combination

In the third experimental setup, the AFG was employed in combination with the Red Pitaya in an attempt to gain a sufficient enough input voltage level, to obtain the resonant peaks. The results obtained from the experiment showed no improvement.



Figure 37: Experiment 3 setup showing the Red Pitaya and AFG combination

4.2.4.4 Experiment 4: Red Pitaya Vector Network Analyser

The fourth experimental setup opted for a different approach to obtain the frequency response of the reactor by utilising the Vector Network Analyser capabilities of the Red Pitaya. The method of using a VNA to measure the frequency response was also done by [6] and [18].

The Vector Network Analyser (VNA) functions by measuring the reflection (amplitude response and phase) of the signal and is generally used for testing filters, amplifiers and antenna design. This reflection occurs as a result of impedance mismatching which is usually undesirable but for this application, it is used to obtain the impedance of the reactor.

In order to use the Vector Network Analyser of the Red Pitaya, an SWR (Standing Wave Ratio) bridge is connected which modifies the measurement system as shown in Figure 39. The SWR bridge is a VNA module (Figure 38) developed by Red pitaya and comes with additional calibration accessories. The SWR bridge is effectively a directional coupler which serves as a means to measure the reflected signal.



Figure 38: Red Pitaya VNA module connected to the Red Pitaya

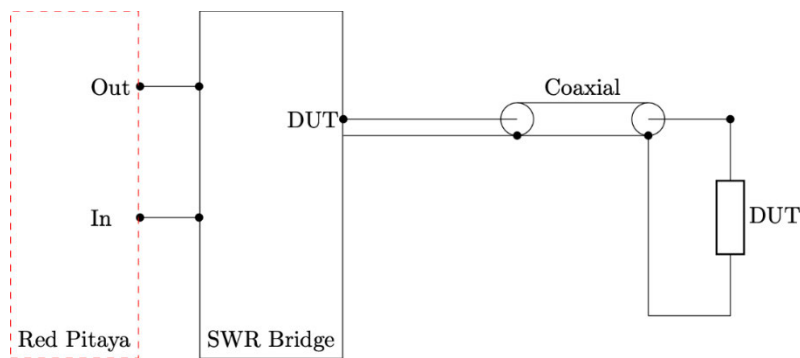


Figure 39: Modified measurement system for impedance measurement

After calibration, the reflected signal was captured by the VNA and showed a clearer frequency response that is similar to the expected characteristic shape depicted in Figure 12. A distinct initial peak could now be seen indicating resonance with clear subsequent peaks showing the capacitive switching as the frequency increases as shown in Figure 41. Resonance occurs at approximately 1.9 MHz which is within reasonable agreement to the expected resonance which was calculated to be 2.32 MHz as they may be external environmental factors affecting the capacitance.

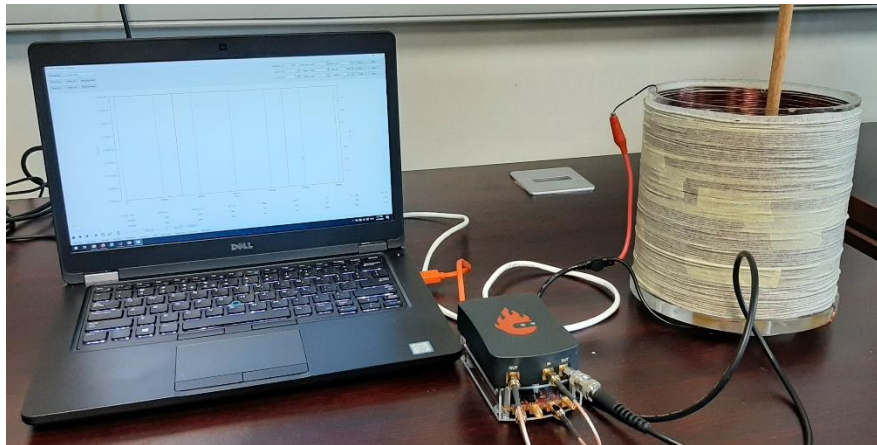


Figure 40: Experiment 4 setup for VNA

4.3 Validation of models

In order to validate the FEM models developed in COMSOL for the two reactors, the results are compared to measured values with the final validation being a comparison of frequency response obtained through simulation compared to a measured frequency response.

Table 13 shows a comparison of measured parameters to the FEM and ECM models developed for Reactor 1. The results show a good correlation with slight discrepancies to the measured. A strong agreement can be seen for the inductance values with a difference of 3.4 μH between the measured and FEM simulated values. It should be noted that the FEM model did not produce an inductance closer to the measured value when compared to the ECM value for inductance. The capacitance differs by approximately 1 pF between the FEM model and the measured capacitance. The FEM model has a circular outer boundary which is grounded which would account for the differences to both the measured and the approximated ECM capacitance. The resistance values are within reasonable margins for the FEM and ECM models with the measured resistance being higher than expected.

Table 13: Table of RLC parameters for Reactor 1 comparing measured, FEM and ECM models

Component	Measured	FEM	ECM
Inductance (μH)	24.2	20.784	23.391
Capacitance (pF)	7.2	8.1784	6.2968
Resistance (Ω)	0.17	0.1930m	0.613m

Table 14 shows a comparison of the calculated RLC parameters to the FEM model developed in COMSOL for Reactor 2. Again, a strong correlation can be seen for the inductance values from both models. The capacitance differs by approximately 1 pF which is most likely due to the same reasons mentioned for Reactor 1.

Table 14: Table of RLC parameters for Reactor 2 comparing FEM and ECM models

Component	FEM	ECM
Inductance (mH)	1.2180	1.3
Capacitance (pF)	4.5813	3.6563
Resistance (Ω)	1.0650	0.3101

Table 15 shows resonance frequencies obtained through simulations of the FEM models compared to computed approximations. Reactor 1 shows very strong agreement while Reactor 2 shows a simulated resonance frequency that is less than satisfactory to what was calculated. This is due to the difference in the capacitance values as mentioned earlier. The resonance frequencies obtained through the ECM model helped guide the FEM modelling by providing an indication that the results were approximately correct, but would require further validation through measurements of the physical reactor.

Table 15: Table comparing FEM resonance frequencies to calculated resonance frequencies

Component	FEM	ECM
Reactor 1 Resonance frequency (MHz)	13.4	13.04
Reactor 2 Resonance frequency (MHz)	1.5	2.32

From all the experiments to measure a frequency response directly from one of the desktop reactors, the frequency response for Reactor 2 using a VNA produced the best results and is compared to the frequency response obtained from the COMSOL model as seen in Figure 41.

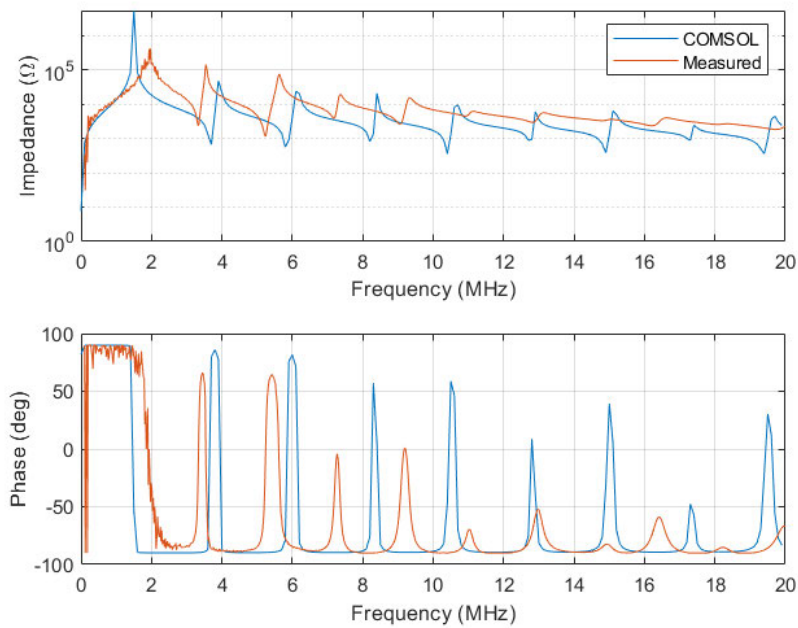


Figure 41: Frequency response and phase comparison between the COMSOL model and VNA measurement for Reactor 2

The resonance frequencies here differ by 0.4 MHz, meaning that the COMSOL model for Reactor 2 shows a good agreement with the measured. Even though the approximated calculated resonant frequency of 2.32 MHz showed poor agreement to FEM simulation, a stronger correlation can be seen between the FEM simulation and measured resonance frequency of 1.5 MHz and 1.9 MHz respectively. The discrepancy between the ECM and FEM here may be due to similar reasons mentioned earlier in this section with respect to the inductance and capacitance specifically.

It can also be clearly observed in Figure 41 that the initial resonance peaks and phase changes are in good agreement with a slight shift between the measured and simulated peaks as the frequency increases. The first point of resonance shows a strong correlation between the measured and simulated frequency responses with the second and third resonance points of resonance occurring at approximately similar frequencies as well. An increase in the difference between the frequency responses is noted as the frequency increases. This may be due to the method of measuring a reflected signal to obtain the frequency response. However, the key point of interest from this comparison is the resonant frequency which shows a good agreement between measured and simulated results.

Reactor 1 model is validated by comparisons to measured and computed values while Reactor 2 is validated by comparing the resonant frequency of the simulated frequency response to measured frequency response from the VNA. Based on the evidence compiled, it can be stated that COMSOL can successfully model Reactor 1 and Reactor 2 using FEM methodologies.

5 Sensitivity Analysis of the Reactor Model

Sensitivity analysis is performed to understand how the inductance, capacitance and resistance are affected by changes such as geometrical/physical changes, the reactor being immersed in liquid coolant as well as changes in resistivity of the copper used. The analysis of the frequency response and LCR values as a result of these changes provides an understanding of factors that should be considered in designing reactors.

5.1 Geometrical Sensitivity Analysis

The FEM model was simulated after scaling the geometry in the z or r direction by +/-10%. Scaling z is equivalent to the length/height of the reactor whilst scaling r refers to the width/diameter of the reactor. The resulting frequency responses are shown and compared to the original. This helps in testing the responsiveness of the model to changes in the geometry.

5.1.1 Length (z scaling)

Scaling the geometry by a factor of 1.1 (+10%) and 0.9 (-10%) resulted in a resonant frequency occurring at 13.5 MHz and 13.2 MHz respectively as shown in the frequency response in Figures- 42 and 43. A drop in the impedance amplitude can be seen for the 0.9 scale factor and the inverse is observed for the scaling by 1.1.

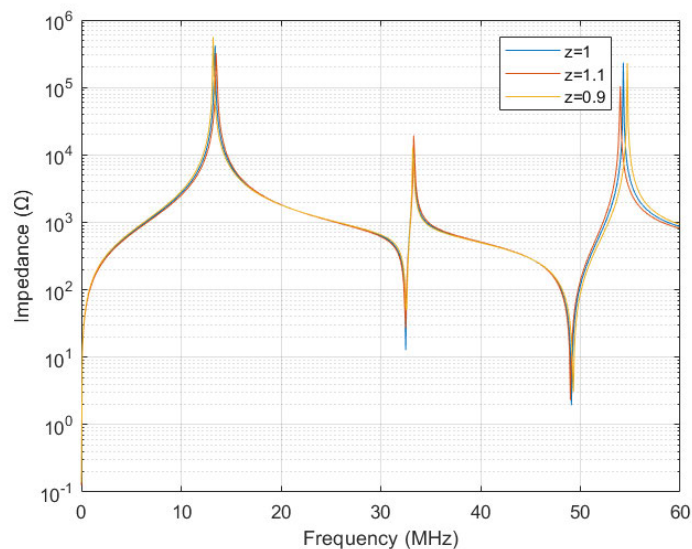


Figure 42: frequency response – z scaling

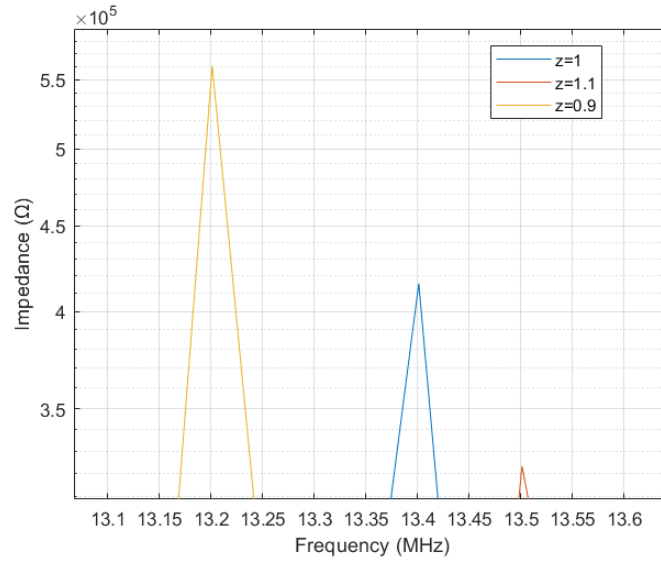


Figure 43: Frequency response - z scaling resonant frequency peak zoom

5.1.2 Width (r scaling)

Scaling the geometry by a factor of 1.1 (+10%) and 0.9 (-10%) resulted in a resonant frequency occurring at 12 MHz and 15.2 MHz respectively as shown in the frequency response in Figures- 44 and 45. A drop in the amplitude can also be noted for width scaling.

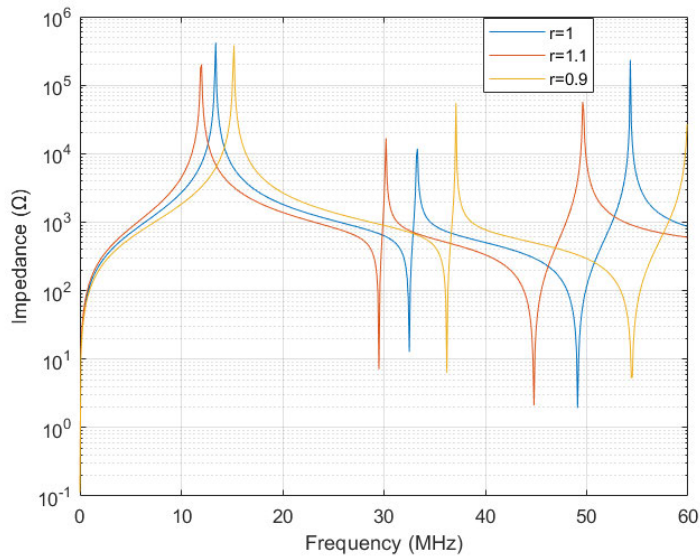


Figure 44: frequency response - r scaling

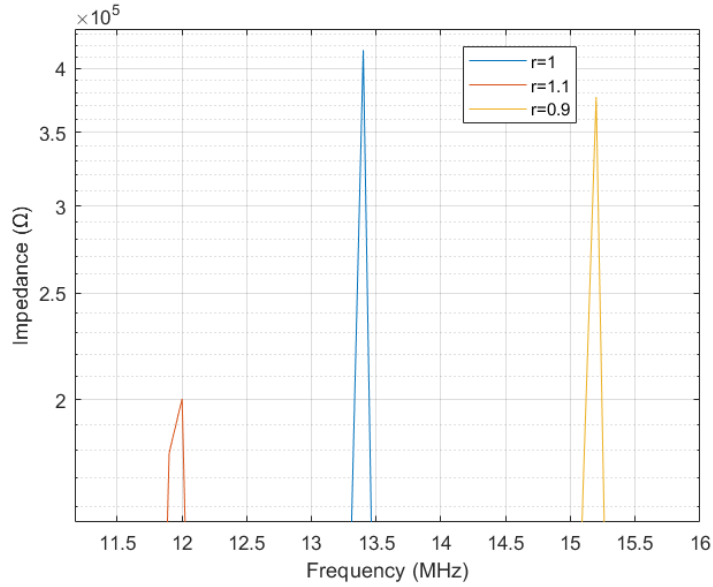


Figure 45: Frequency response - r scaling resonant frequency peak zoom

5.1.3 Summary of Geometrical Sensitivity Analysis

Noting that the original resonance frequency occurred at 13.4 MHz, it can be observed from Figures-43 and 45 that the resonance frequency has a direct proportionality relationship to changes in the length of the device and an inverse proportionality to the changes in width. Increasing the length of the device by 10% showed an increase in the resonance frequency by 0.75% and a decrease by 1.49% when the length was reduced by 10%. Conversely, when the width of the device was increased by 10%, the resonant frequency decreased by 10.45% and increased by 13.43% when the width was decreased 10%. It can also be seen that the width has more of an effect on the resonance frequency of the device than the length. These changes are expected as geometrical changes to a reactor directly affects the inductance, resistance and capacitance.

Table 16 shows a comparison of the RLC parameters at different scales to the original values at 1 kHz in order to understand the influence of the geometry on the parameters.

Table 16: RLC parameters at 1 kHz for structural scaling of reactor

Parameters	Original	Z scaling		R scaling	
		+10%	-10%	+10%	-10%
Resistance (mΩ)	0.1930	0.1741	0.2164	0.2006	0.1857
Inductance (μH)	20.784	19.963	21.656	23.589	17.995
Capacitance (pF)	8.1784	8.5759	8.5422	8.2568	7.4456

Resistance of the coil has direct proportionality to the diameter of the coil and inverse proportionality to the diameter of the conductor as per equations (11) and (12). When scaling in the z axis by 10%, a reduction can be seen. This is because the cross-sectional area of the conductor has increased but the diameter of the coil has not changed. When scaled in the radial axis, the resistance increases despite the increase in the cross sectional area of the conductor since the diameter has increased too. The converse of this is true for scaling by -10% in the z and r axis.

The inductance according to equation (10) is directly proportional to the diameter of the reactor and inversely proportional to the length. From the results in Table 16, this can be seen to be true as the inductance reduces when the reactor is scaled by 10% in length and increases when scaled by -10%. As scaling r directly increases and decreases the diameter of the reactor, the inductance increases and decreases for scaling 10% and -10% respectively, which agrees with equation (10).

From equation (2), it can be established that capacitance is directly proportional to the diameter of the reactor as well as the diameter of the conductor but inversely proportional to the length of the reactor. This agrees with the simulated results as the capacitance increases and decreases when scaled on the r axis by 10% and -10% respectively. When scaled by length, only an increased capacitance is observed.

5.2 Liquid Nitrogen Insulation

This section involves simulating the FEM model under conditions that would replicate the reactor being immersed in liquid nitrogen. The purpose of this is to observe the effects that a change in the insulation medium used, that is air to liquid nitrogen, would make to the capacitance of the reactor and to see if it can be modelled correctly. The relative permittivity used was 1.45 which resulted in the frequency response shown in Figures- 46 and 47. The resonance frequency is observed to occur at 11.5 MHz which is 14.18% lower than the original resonance frequency.

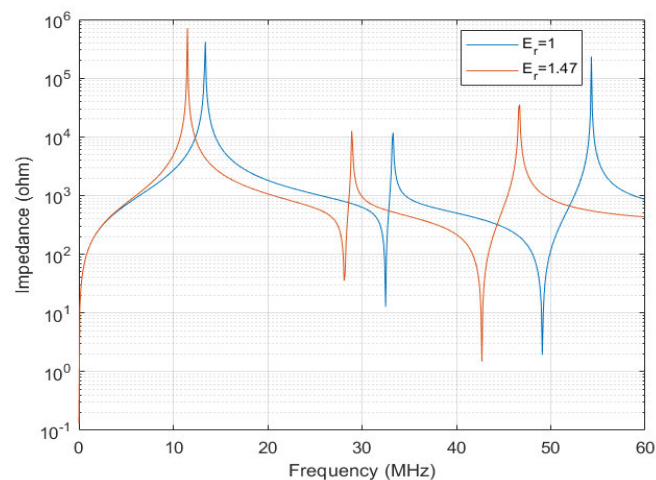


Figure 46: Frequency response comparison - liquid nitrogen

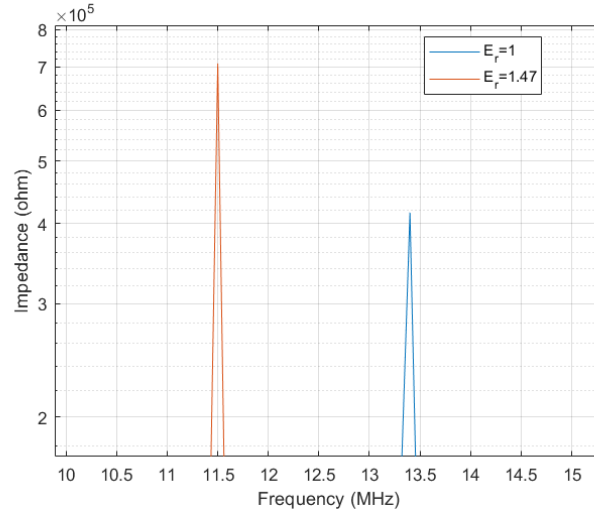


Figure 47: Frequency response comparison - liquid nitrogen resonant frequency zoom

The reduction in the resonance frequency is a direct result of the increase in capacitance as seen in Figure 47. Capacitance changed from 8.2457 pF in air, to 0.1047 pF in liquid nitrogen at 1 kHz which is expected as the equation for capacitance (2) shows a direct correlation of capacitance to the relative permittivity of the medium. The medium in which the reactor is immersed is an important factor for these reasons.

5.3 Resistivity of Copper

Immersing a reactor in liquid nitrogen would affect the temperature and subsequently the resistivity of the winding. To analyse the effect that changes in the resistivity of copper would have on the model, the conductivity was altered accordingly to emulate copper at a temperature of approximately 77 K, i.e. temperature of liquid nitrogen, it's boiling point. A temperature dependant conductivity is given by equation (24) as per the COMSOL documentation [33],

$$\sigma = \frac{1}{\rho_0(1 + \alpha(T - T_{ref}))}, \quad (24)$$

where ρ_0 , α , T and T_{ref} represent the resistivity, temperature coefficient of resistance, temperature and reference temperature of the material respectively.

Based on equation (24), conductivity in terms of temperature shows an inverse relationship between conductivity and temperature.

Figure 48 is a comparison of the conductivity of copper under normal conditions ($T = 300$ K, $\sigma = 5.988e7$) and the approximate conductivity of copper when in liquid nitrogen ($T = 77$ K, $\sigma \approx 5.988e9$).

As expected, a reduction in the maximum impedance can be seen in Figure 48, when the conductivity is increased. The resonance frequency is observed to be the same for both.

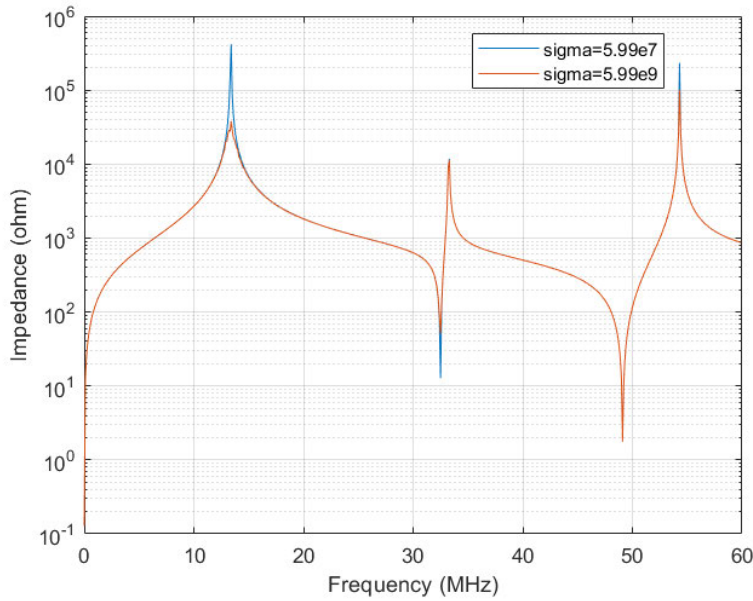


Figure 48: Impedance comparison for $T = 300 \text{ K}$ and $T = 77 \text{ K}$

By reducing the resistivity of copper, one would expect to see a reduction in the impedance as well as an increase in the current density. This can be further explained by equation (25) for surface current density of a cylindrical conductor [34],

$$J_r = a_0[ber(mr) + jbei(mr)], \quad (25)$$

where

$$ber(mr) = 1 + \frac{(mr)^4}{2^2 4^2} - \frac{(mr)^8}{2^2 4^2 6^2 8^2} + \dots, \quad (26)$$

$$bei(mr) = -\frac{(mr)^2}{2^2} + \frac{(mr)^6}{2^2 4^2 6^2} - \frac{(mr)^{10}}{2^2 4^2 6^2 8^2 10^2} + \dots, \quad (27)$$

and

$$mr = \sqrt{\omega\sigma\mu} * r, \quad (28)$$

Equations (26) and (27) represent the real and imaginary solutions using Bessel's Equation and α_0 represents a constant for surface current density. In order to understand the effects of conductivity on current density for the copper wire, equation (28) is plotted against frequency in Figure 49 where ω , σ , μ and r represent the angular frequency, conductivity, permeability and cross-sectional radius of the conductor. This is done since equation 28 has direct proportionality to the current density and accounts for the conductivity, making it a good indicator. An exponential increase can be seen when the conductivity is increased which in turn implies such an increase for the current density.

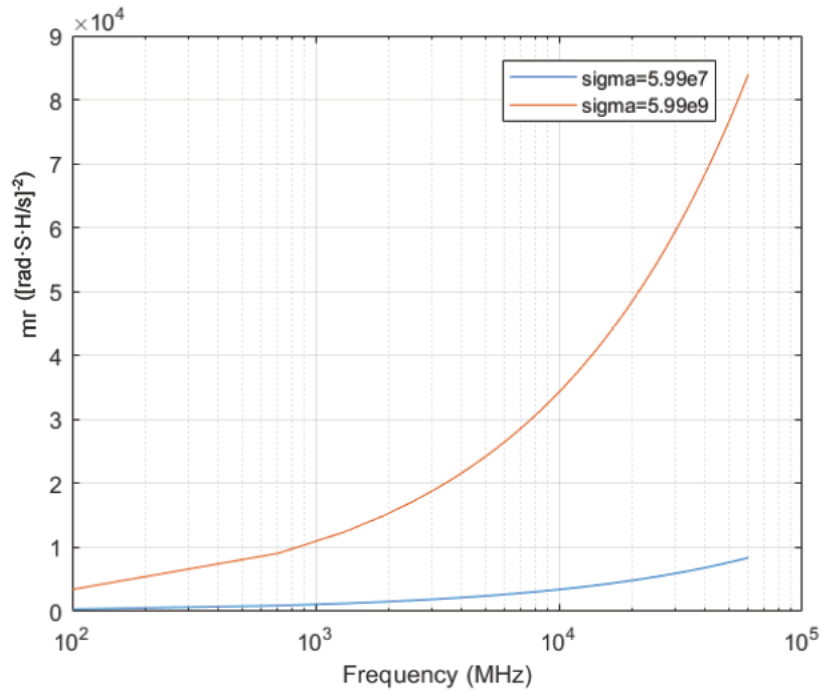


Figure 49: Comparison of approximate effect of conductivity on mr

Considering the effects on skin depth, an increase in conductivity (decrease in resistivity) would imply a decrease in the skin effect as per equation (15) which shows a direct proportionality relationship to resistivity. Figure 50 shows the simulations from the FEM model which exhibit the current density increasing when increasing conductivity from (a) 5.988×10^7 to (b) 5.988×10^9 . Skin and proximity effects can also be seen as the current density is weakest at points that are closest to adjacent conductors.

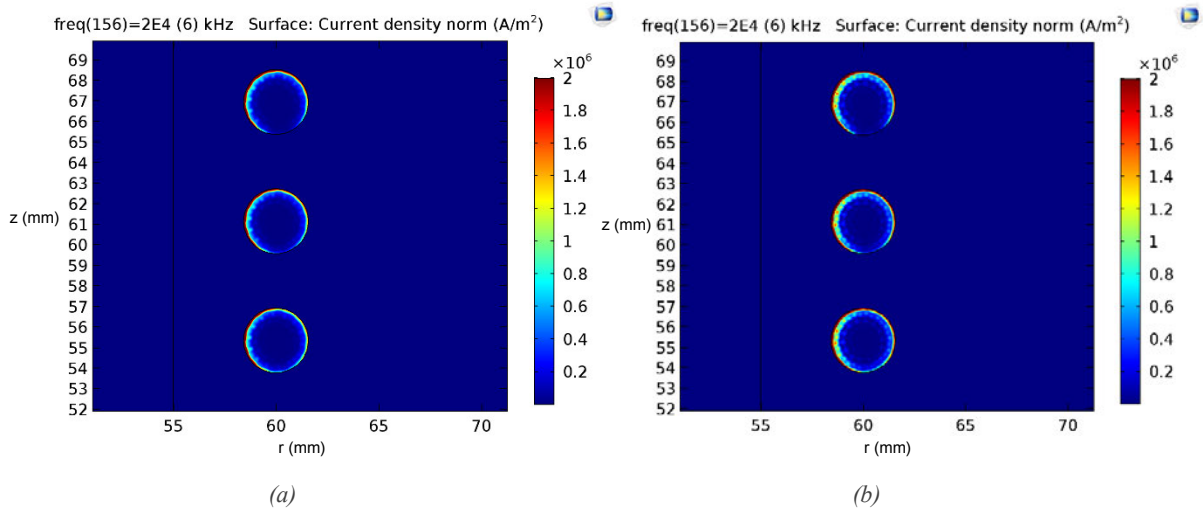


Figure 50: Comparison of current density where (a) $T = 300\text{ K}$ and (b) $T = 77\text{ K}$

Full-Scale Reactor

The simulation results for a full-scaled reactor are documented in this section to show that the COMSOL model can be extrapolated to accurately model a full-scaled reactor. The FEM model is geometrically modified as per the design specifications for a prototype SSR from Khan et al [1] and is a scaled version of the desktop reactor. The aim of this is to verify that the FEM model would still produce valid results when scaled. Note, the simulations done are for a full scale reactor with copper windings and not that of superconducting material.

5.4 Full-Scale Reactor Geometry

The parameters for the full-scaled reactor are tabulated in Table 17 and the modified geometry of the FEM model can be seen in Figure 51.

Table 17: Table of dimensions of a full scale reactor

Parameter	Value
Outer diameter of former	0.85 m
Inner diameter of former	0.46 m
Height of reactor	0.86 m
Number of turns	66
Distance between turns	13 mm
Conductor radius	3.15 mm

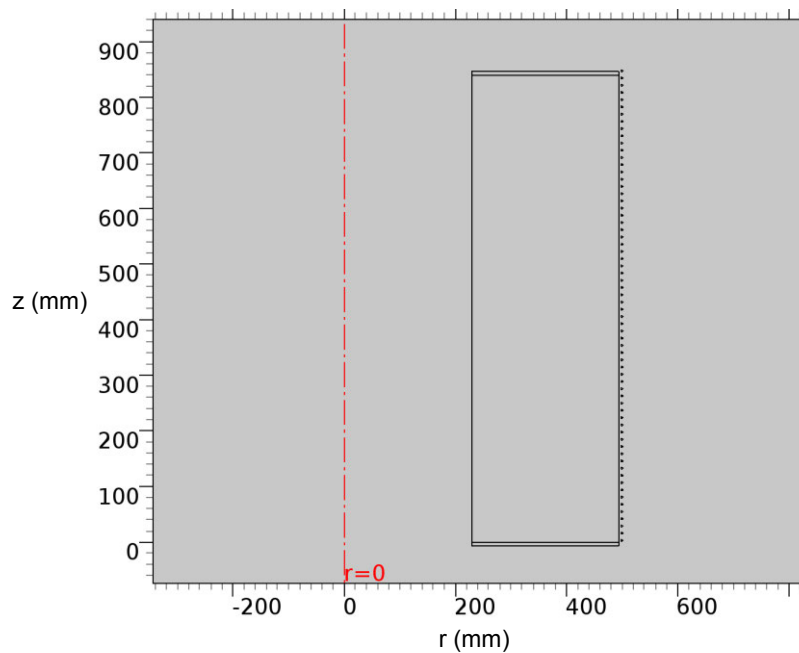


Figure 51: FEM geometry for full scale reactor

5.5 FEM Simulation Results

The FEM model solved for frequencies between 1 kHz to 10 MHz in steps of 10 kHz. The results in Table 18 were taken at a frequency of 1 kHz.

Table 18: FEM results for a full-scaled reactor at 1 kHz

Parameter	Simulated
Inductance (mH)	2.28
Capacitance (pF)	165
Resistance (m Ω)	0.315
Resonant Frequency (kHz)	380

The expected inductance for these geometrical values is 2.24 mH as stated in [1], hence the simulated inductance agrees with the expected inductance and calculated inductance of 2.5 mH.

The resonance frequency can be seen to occur around 380 kHz in Figure 52 with the approximated resonance calculated to occur around 530 kHz. However, as seen with Reactor 2, it has been established that the FEM model produces results much closer to actual measured results than the calculated values.

What we can observe from Figure 52 is that by scaling the reactor, we observe a much smaller resonance frequency, meaning that power systems would be at risk with transients that occur at lower frequencies as well. The geometrical parameters involved in designing reactors is of great importance for this reason.

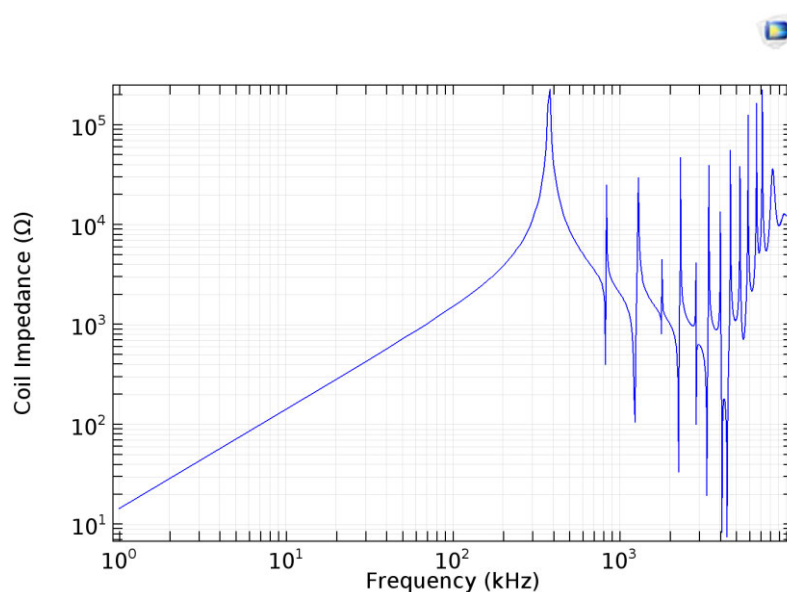


Figure 52: Impedance frequency response of the full-scale reactor

6 Conclusion

Reactors are subject to various transients in the power system (switching or lightning). Modelling the frequency response of the reactor would be important to identify any characteristics of interest or design issues that would need to be considered, particularly related to the case where reactors are immersed in a liquid dielectric and significantly cooled.

The conclusions for this dissertation's research questions are as follows.

Can the frequency response of the desktop reactor be modelled and analysed by employing FEM methodologies through COMSOL software? Chapter 3 documents the modelling process in COMSOL Multiphysics for two reactors with the guidance of calculated values for the inductance, resistance, capacitance and resonant frequencies of these reactors. The effect of different mesh settings in COMSOL was also investigated and it was found that the extra-fine and extremely-fine mesh settings showed a minimal change (0.75%) in the frequency response. Based on the findings, it was decided that the simulations be done using the extremely-fine mesh setting. The frequency response obtained from the FEM models in Figure 21 and 26 agreed with research from past studies as seen in Figure 12 in terms of the characteristic shape. Inductive, resistive and capacitive components for both reactors were recorded too.

Chapter 4 then sought to further validate these models through measurements of the actual reactors. The FEM model for Reactor 1 was validated by comparing the inductance, resistance and capacitance obtained from COMSOL, to the measured values which used an LCR meter. The inductance here differed by 3.4 μH and the capacitance by 1 pF compared to the measured values. A strong agreement was seen between FEM results from COMSOL and the measured results from the LCR meter.

The FEM model for Reactor 2 was validated by comparing the frequency response obtained from COMSOL to a measured frequency response using a Vector Network Analyser. The agreement seen with the first 3 resonant frequencies proved a strong case of validation for this model with the initial resonance frequencies differing by 0.4 MHz. It was clear that the FEM model was in closer agreement to the measured than the calculated values as well. A noteworthy point is the increase in differences between peaks as the frequency increased which indicated the error increasing with frequency. This could be due to the measurement method of measuring a reflected signal. This chapter also highlighted the difficulties faced in correctly measuring the frequency response to clearly depict resonant peaks.

What factors or parameters in terms of resistance, capacitance and inductance would affect performance of a fault limiting reactor under transients? Chapter 5 performed a sensitivity analysis on the FEM models with respect to geometrical sensitivity, liquid nitrogen insulation (liquid dielectric) and altering the resistivity of copper to emulate a significantly cooled reactor.

The geometrical sensitivity analysis showed the physical changes have a far greater impact on the inductance of the reactors as compared to the capacitance and resistance. This would expectedly affect the frequency response with radial changes of the reactor causing a more significant shift in the resonance peaks than height changes. A reduction in the radius showed an increase in the resonant frequency and vice-versa.

For the case of the reactor being immersed in a liquid dielectric, the permittivity was increased to match that of liquid nitrogen, i.e. 1.45. As expected from the frequency response, the resonant frequency occurred at a significantly lower point (14.18% lower than the original resonance frequency) due to the increase in capacitance. It is for this reason that reactor designers should take extra precaution when choosing a liquid dielectric for a current limiting reactor. Liquid nitrogen does have a higher breakdown voltage than air which is an additional advantage that should be considered as well.

The attempt to examine the effects of a significantly cooled air-core reactor involved reducing the resistivity of copper significantly, or increasing the conductivity significantly. This did not cause any significant shift in the resonant frequencies but there was an expected drop in the maximum impedance at resonant frequency. A more condensed current density was observed in the conductor coil. The equation for surface current density substantiated this point when considering the effects of conductivity.

What models can be used to accurately represent a reactor and can it be extrapolated to represent a full-scale reactor? A full scale copper-wire reactor was modelled using FEM through COMSOL Multiphysics in Chapter 6 and the results examined. The physical parameters of this reactor were based on the reactor designed by Khan et al [1]. The inductance of 2.28 mH obtained through FEM showed a close correlation with the expected value of 2.24 mH and the resonance was determined to be 380 kHz.

This FEM based approach is ideal for modelling desktop reactors and thereafter scaling it for full-sized reactors as it is far easier and user friendly to implement the scaling process of the geometry in COMSOL as compared to other methods which involve tedious calculations.

6.1 Recommendations

The next steps for this project would be to model the Superconducting Series Reactor to investigate if the expected change in coil material can be correctly modelled in COMSOL Multiphysics. This dissertation would provide the developers of the SSR with an idea of what design considerations should be taken when designing an SSR with regards to factors that would affect the capacitance of the reactor.

7 References

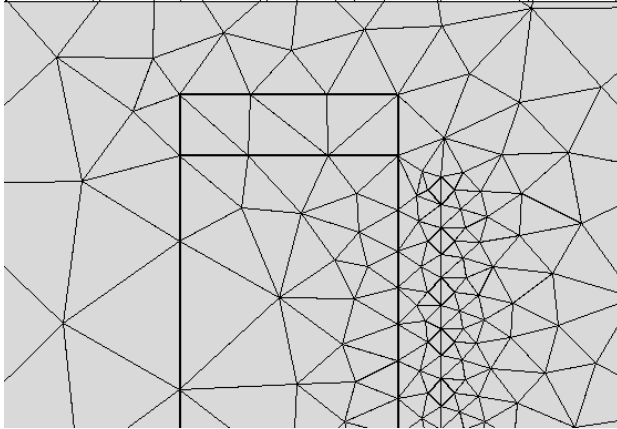
- [1] M. F. Khan, A. L. L. Jarvis, E. A. Young, A. G. Swanson, J. C. Archer and G. R. Stephen, "The novel design of an energy efficient superconductorbased series reactor for installation at a grid connected research site," *Journal of Energy in South Africa*, vol. 31, no. 2, pp. 19-33, 2020.
- [2] M. J. Heathcote, "Modern power station practice," in *Electrical Systems and Equipment*, London, Pergamon Press, 1992, pp. 276-278.
- [3] K. Papp, M. R. Sharp and D. F. Peelo, "High voltage dry-type air-core shunt," *CIGRE*, Vols. A3-101, pp. 349-354, 2014.
- [4] S. Ejaz and S. Anwar, "Voltage distribution along reactor winding under very fast transients," Chalmers University of Technology, Gothenburg.
- [5] P. S. R. Murty, "Chapter 11- Short circuit analysis," in *Power Systems Analysis*, BS Publications, 2017, pp. 277-312.
- [6] M. Enohnyaket, "PEEC modeling and verification for broadband analysis of air-core reactors," *IEEE Transactions on Power Delivery*, vol. 24, no. 2, pp. 719-729, 2007.
- [7] K. Schon, "Introduction," in *High Impulse Voltage and Current Measurement Techniques*, Switzerland, Springer, 2013, p. 1.
- [8] S. V. Kulkarni and S. A. Khaparde, "Surge phenomena in transformers," in *Transformer Engineering Design and Practice*, New York, Marcel Dekker, Inc., 2004, pp. 277-314.
- [9] H. Wheeler, "Simple inductance formulas for radio coils," *Proceedings of the Institute of Radio Engineers*, vol. 16, no. 10, pp. 1398 - 1400, 1928.
- [10] C. R. Paul, "'Loop' inductance vs. 'Partial' inductance," in *Inductance: Loop and Partial*, New Jersey, John Wiley & Sons, Inc., 2010, p. 8.
- [11] H. Johnson and M. Graham, "Skin effect; proximity effect," in *High-Speed Signal Propagation: Advanced Black Magic*, Prentice-Hall PTR, 2003, pp. 58-63, 79-87.
- [12] M. Enohnyaket and J. Ekman, "Analysis of air-core reactors from DC to very high frequencies using PEEC models," *IEEE Transactions on Power Delivery*, vol. 24, no. 2, pp. 5-6, 2009.

- [13] W. M. Middleton and M. E. Van Valkenburg, "Fundamentals of networks," in *Reference Data for Engineers (Ninth Edition)*, Newnes, 2002, pp. 6-6-6-7.
- [14] B. J. van Jaarsveld, "Wide band modelling of an air-core power transformer winding," Stellenbosch University, Stellenbosch, 2013.
- [15] I. F. Kováčević, A. Müsing and J. W. Kolar, "PEEC modelling of toroidal magnetic inductor in frequency domain," *The 2010 International Power Electronics Conference - ECCE ASIA* -, pp. 3158-3165, 2010.
- [16] K. Naishadham, "Closed-form design formulas for the equivalent circuit characterization of ferrite inductors," *IEEE Transactions on Electromagnetic Compatibility*, vol. 53, no. 4, pp. 923-932, 2011.
- [17] CIGRE JWG A2/C4.39, "Case study #12: High-frequency modelling of a 500 KV transformer – detailed model vs. simplified model," *Electrical Transient Interaction Between Transformers and the Power System – Part 2: Case Studies*, pp. 106-112, 2014.
- [18] CIGRE JWG A2/C4.39, "Transformer modelling," *Electrical Transient Interaction Between Transformers and the Power System – Part 1: Expertise*, pp. 33-56, 2014.
- [19] M. Popov, "General approach for accurate resonance analysis in Transformer Windings," *Electric Power Systems Research*, vol. 161, pp. 45-51, 2018.
- [20] S. Wang, Z. Guo, T. Zhu, H. Feng and S. Wang, "A new multi-conductor transmission line model of transformer winding for frequency response analysis considering the frequency-dependent property of the lamination core," *Energies*, vol. 11, no. 4, p. 826, 2018.
- [21] C. Banda and J. Coller, "Measurement of switching surges and resonance behaviour in transformer windings," SAUPEC, 2015.
- [22] Y. Shibuya, S. Fujita and E. Tamaki, "Analysis of very fast transients in transformers," *Generation, Transmission and Distribution, IEEE Proceedings*, vol. 148, no. 5, pp. 377-383, 2001.
- [23] M. Popov, L. van der Sluis, G. C. Paap and H. De Hert, "Computation of very fast transient overvoltages in transformer windings," *IEEE TRANSACTIONS ON POWER DELIVERY*, vol. 18, no. 4, pp. 1268-1274, 2003.

- [24] H. A. Hamid, "Transients in reactors for power systems compensation," School of Engineering Cardiff University, Cardiff, 2012.
- [25] T. S. Tran, G. Meunier, P. Labie, Y. L. Floch, J. Roudet, J. M. Guichon and Y. Maréchal, "Coupling PEEC-finite element method for solving electromagnetic problems," *IEEE Transactions on Magnetics*, vol. 44, no. 6, pp. 1330-1333, 2008.
- [26] Massachusetts Institute of Technology, "Finite Element Method," 2004. [Online]. Available: http://web.mit.edu/16.810/www/16.810_L4_CAE.pdf.
- [27] B. Vahdi, M. Eslamian and S. Hosseinian, "Transient simulation of cast-resin dry-type transformers using FEM," *European Transactions on Electrical Power*, vol. 21, pp. 363-379, 2010.
- [28] D. Patel and D. Rajput, "Analysis & simulation of 25 KVA distribution transformer design using FEMM," *International Journal of Advanced Research in Electrical, Electronics and Instrumentation Engineering*, vol. 6, no. 3, pp. 1279-1285, 2017.
- [29] K. R. Hameed and I. J. Jabur, "FEM application for evaluating and improving the insulation system of the 33 kV wound-core type distribution transformer," *Modern Applied Science*, vol. 12, no. 9, pp. 39-56, 2018.
- [30] M. L. Myint and Y. A. Oo, "Analysis of distribution transformer design using FEA," *International Journal of Scientific Research Engineering & Technology*, vol. 3, no. 4, pp. 773-775, 2014.
- [31] H. Benguesmia, N. M'Ziou and A. Boubakeur, "Simulation of the potential and electric field distribution on high voltage insulator using the finite element method," *Diagnostyka*, vol. 19, no. 2, pp. 41-52, 2018.
- [32] X. Luo, S. Wang, Y. Wang and Y. Gu, "Analysis of a dry-type reactor fault based on COMSOL thermal field simulation and high frequency pulse oscillations," *MATEC Web of Conferences*, vol. 173, no. 2, pp. 02-27, 2018.
- [33] COMSOL, "The magnetic and electric fields interface," *AC/DC Module User's Guide*, pp. 233-261, 2015.
- [34] J. P. Reynders, "Resistance," *Electrical Parameters of Power Lines*, p. 15, 2006.

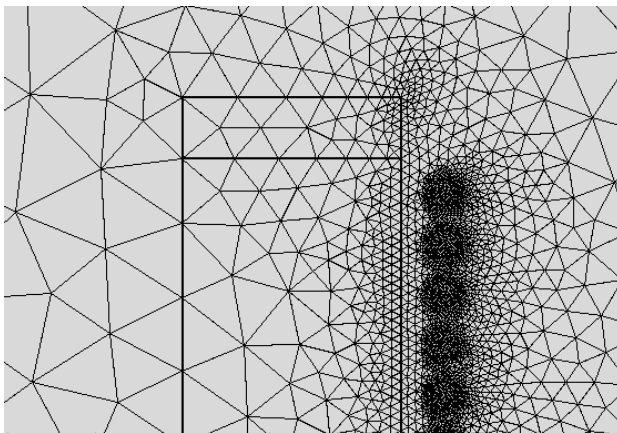
Appendix A1 – Extra-coarse mesh

The image below shows COMSOL's extra-coarse mesh setting applied to a portion of the geometry of Reactor 1 with the main purpose being to show that the conductors are not correctly represented.



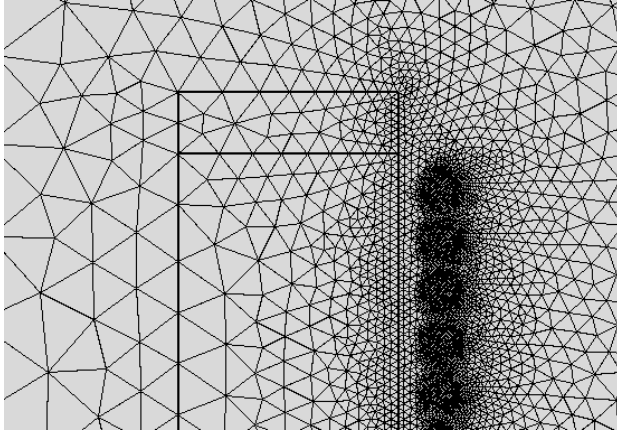
Appendix A2 – Normal mesh

The image below shows COMSOL's normal mesh setting applied to a portion of the geometry of Reactor 1. Note the conductors/circular geometries are more accurately depicted.



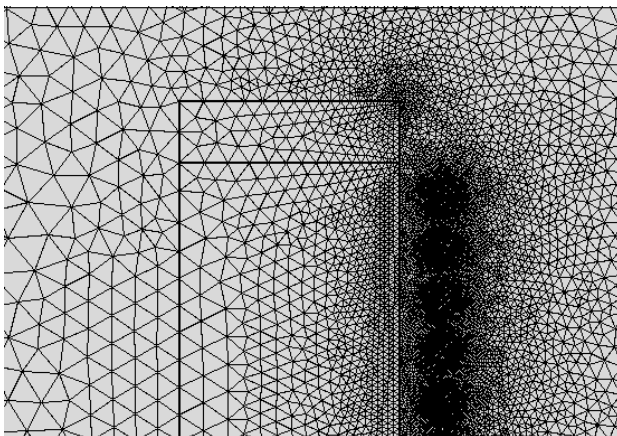
Appendix A3 – Extra-fine mesh

The image below shows COMSOL's extra-fine mesh setting applied to a portion of the geometry of Reactor 1. Note the increase in the number of elements as compared to a Normal and extra-coarse mesh setting.



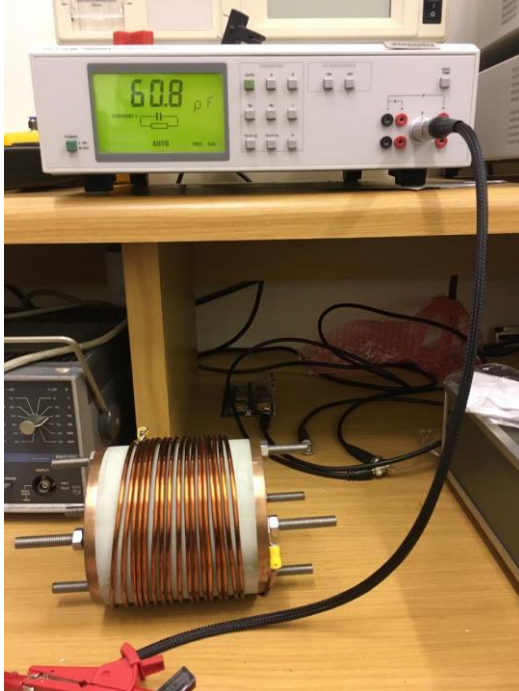
Appendix A4 – Extremely-fine mesh

The image below shows COMSOL's extra-fine mesh setting applied to a portion of the geometry of Reactor 1. Note a further increase in the number of elements as compared to the extra-fine mesh setting.



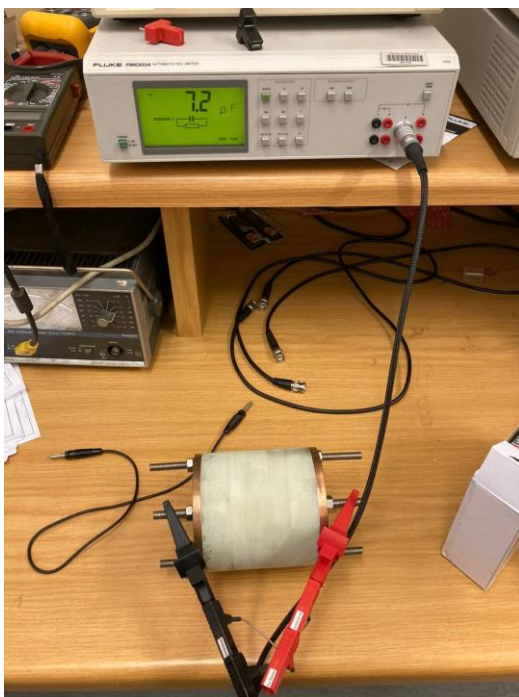
Appendix B1 – Capacitance of cable for measurements

The image below depicts the measurement of the capacitance of the cable used, to measure the inductance, capacitance and resistance of Reactor 1.



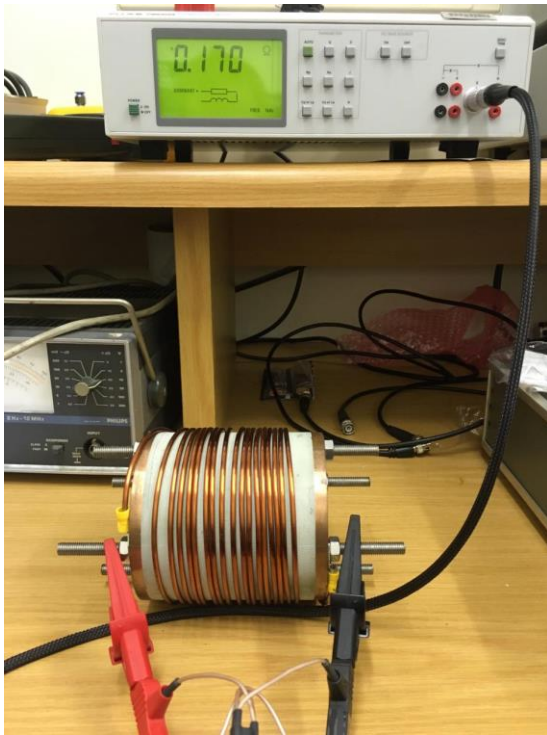
Appendix B2 – Capacitance of desktop reactor

The image below depicts the measurement of the capacitance of Reactor 1 at 1 kHz.



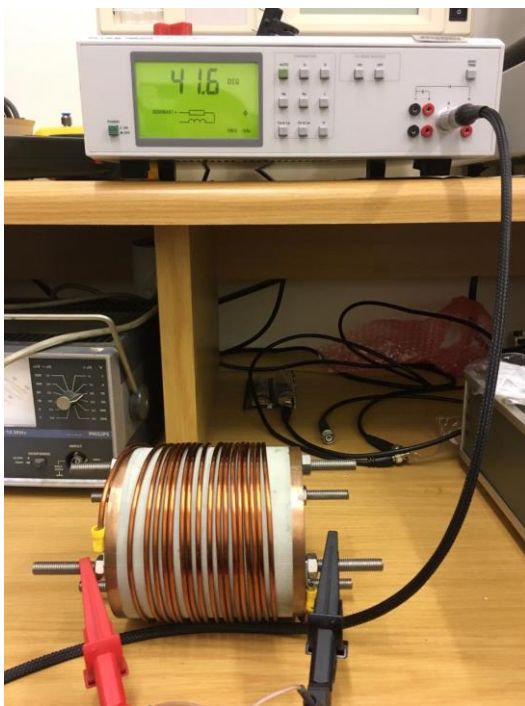
Appendix B3 – Resistance measurement for the desktop reactor

The image below depicts the measurement of the resistance of Reactor 1 at 1 kHz.



Appendix B4 – Phase angle measurement for the desktop reactor

The image below depicts the measurement of the phase angle of Reactor 1 at 1 kHz.



Appendix C – MATLAB code RLC calculations

MATLAB Script for calculating Inductance, Resistance, total Capacitance and Resonant frequency of Reactor 2. The same code is used to calculate the parameters for Reactor 1 after adjusting the input variables accordingly.

```
clear;

N = 100;           % Number of turns
Do = 0.180;       % Outer diameter (m)
Di = 0.174;       % Inner diameter (m)
rcond = 3.15e-3;  % Radius of conductor (m)
l = 0.17;         % Height of reactor (m)
rho = 1.68e-8;    % Resistivity of copper (Ohm.m)
eps0 = 8.85e-12;  % Permittivity of free space
eps_r = 5;        % Permittivity of resin
ts = 0.4e-3;      % Space between coils (m)
eps_c = 3.2;      % Permittivity of copper coating
eps_air = 1;      % Permittivity of air
d = 0.3;          % Distance from coil to ground plane (m)

% Wheeler's Formula for inductance (H)
Lcore = (Do*100)^2*N^2/(45*Do*100+100*l*100)*1e-6;

% DC resistance(Ohm)
Rwind = (Do+rcond)*pi*rho/(pi*rcond^2);

Al = (Do/2)^2*pi; % (m^2)
% area of dielectric (m^2)
Ac = Al-(Di/2)^2*pi;

% Capacitance of dielectric core (F)
Ccore = eps_r*eps0*Ac/l;

% Capacitance between turns (F)
Ct1 = ((eps0*eps_c*pi*Do*(rcond+ts))/ts);

% Series Capacitance (F)
Cs1 = Ct1/N;

% Capacitance to ground plane (F)
Cg_t = (eps0*2*pi*(l)/acosh(d/rcond));

% Total capacitance (F)
C_tot = (Cs1)+Cg_t+Ccore;

% Resonant frequency (Hz)
f_Res = 1/(2*pi*sqrt(Lcore*C_tot));
```

Appendix D – MATLAB code SFRA

MATLAB code for Sweep Frequency Response Analyser.

```
% Define Red Pitaya as TCP/IP object
clear all
close all
clc
IP= '169.254.167.132'; % Input IP of your
Red Pitaya... % If you are using
port = 5000; % If you are using
WiFi then IP is: % 192.168.128.1
tcpipObj=tcpip(IP, port); % 192.168.128.1
    tcpipObj.InputBufferSize = 16384*32;
    tcpipObj.OutputBufferSize = 16384*32;

%% Open connection with your Red Pitaya
fopen(tcpipObj);
tcpipObj.Terminator = 'CR/LF';
flushinput(tcpipObj)
flushoutput(tcpipObj)

%% Setting generator output1

fprintf(tcpipObj, 'OUTPUT1:STATE ON'); % Set output1 to ON
fprintf(tcpipObj, 'SOUR1:FUNC SQUARE'); % Set function of
output signal {sine, square, triangle, sawu, sawd, pwm}
fprintf(tcpipObj, 'SOUR1:FREQ:FIX 1000'); % Set frequency of
output signal
fprintf(tcpipObj, 'SOUR1:VOLT 0.5'); % Set amplitude of
output signal
fprintf(tcpipObj, 'SOUR1:VOLT:OFFS -0.017'); % Set Offset of
generator

%% Acquire data from oscilloscope

fprintf(tcpipObj, 'ACQ:RST'); % Can be 'ACQ:RST'
or 'ACQ:STOP'??
fprintf(tcpipObj, 'ACQ:DEC 8'); % Set decimation
function
fprintf(tcpipObj, 'ACQ:TRIG:LEV 0'); % Set trigger level in
mV
fprintf(tcpipObj, 'ACQ:TRIG:DLY 4100');

fprintf(tcpipObj, 'ACQ:START');
pause(0.1)

fprintf(tcpipObj, 'ACQ:TRIG CH1_PE');
% Wait for trigger
% Until trigger is true wait with acquiring
% Be aware of while loop if trigger is not achieved
% Ctrl+C will stop code executing in Matlab

while 1
    trig_rsp=query(tcpipObj, 'ACQ:TRIG:STAT?');
```

```

    if strcmp('TD',trig_rsp(1:2)) % Read only TD

        break

    end
end

%% Read data from buffer

signal_str1=query(tcpipObj,'ACQ:SOUR1:DATA?');
signal_str2=query(tcpipObj,'ACQ:SOUR2:DATA?');

% Convert values to numbers.% First character in string is "{"
% and 2 latest are empty spaces and last is "}".

signal_num1=str2num(signal_str1(1,2:length(signal_str1)-3))+0.498;
signal_num2=str2num(signal_str2(1,2:length(signal_str2)-3))+0.498;
num1=signal_num2+0.0105;

%% For plotting signal in respect to time you can use code below

fs = query(tcpipObj,'ACQ:SRA:HZ?') % Get sampling rate in
string
Fs = sscanf(fs,'%f Hz',[2,inf]) % Get sampling rate in
number
buffer_ln=16384; % Buffer size

% Create time vector in respect to decimation value
% Each decimation value has its own time length of buffer
% therefore must select correct time scale for each decimation value

% t=0:buffer_ln/Fs:buffer_ln/Fs*(buffer_ln-1);
% t=0:8E-9:8E-9*(buffer_ln-1); % for 1
t=0:6.402587891E-8:6.402587891E-8*(buffer_ln-1); % for 8
% t=0:5.120239258E-7:5.120239258E-7*(buffer_ln-1); % for 64
% t=0:8.192016602E-6:8.192016602E-6*(buffer_ln-1); % for 1024
% t=0:6.555175781E-5:6.555175781E-5*(buffer_ln-1); % for 8192
% t=0:5.242919922E-4:5.242919922E-4*(buffer_ln-1); % for 65536

% figure,plot(t,signal_num1);
% xlabel('time (s)');
% ylabel('voltage (V)');
% grid on
% figure,plot(t,num1,'red');
% xlabel('time (s)');
% ylabel('voltage (V)');
% grid on
figure(1),plot(t,signal_num1,t,num1);
xlabel('time (s)');
ylabel('voltage (V)');
grid on

%% Reset to default values

```

```
fprintf(tcpipObj, 'ACQ:RST');  
fprintf(tcpipObj, 'GEN:RST');  
fclose(tcpipObj)
```